Chapter 10

Novel Optical Device Materials – Molecular-Level Hybridization

Kyung M. Choi

Additional information is available at the end of the chapter

http://dx.doi.org/10.5772/50032

1. Introduction

Silicate glass has been widely used for optical device materials due to its excellent optical transparency. To satisfy our multiple demands in advanced optical device materials, organic/inorganic hybrid composites have been widely prepared by a bulk mixing technique, which is physically mixing multiple components at the bulk scales.

However, conventional glassy materials have shown limitations to modify their physicochemical properties by inserting desired components into glassy hosts. In addition, a significant phase separation occurs during a mixing process of multiple components, especially immiscible phases.

To overcome those limitations, there are growing interests in doping organic components or semiconductor particles into glassy hosts without any phase separation to combine beneficial properties at the molecular scales, and thus to bring desired properties (Figure 1). [1]

Hybrid materials lie at the interface of the organic and inorganic material regimes, where versatility in molecular tailoring approach offers novel molecular modifications in design of new chemical structures. Hybrid materials can also range, depending on the method of formation and domain size, from physical mixtures of inorganic oxides and organics (blends, composites) to nanocomposites and molecular composites that utilize formal chemical linkages between the organic and inorganic domains on the molecular scale.

Hybrid materials are ranged from the bulk-scales to molecular scales as shown in Figure 2 to mix up multiple components. [1-10]

Usually, hybrid materials mixed at the bulk scales retain the original properties of the individual organic and inorganic components. In other words, their final properties are significantly influenced by the characteristics and their domain sizes of individual components after the mixing process at the bulk scales.

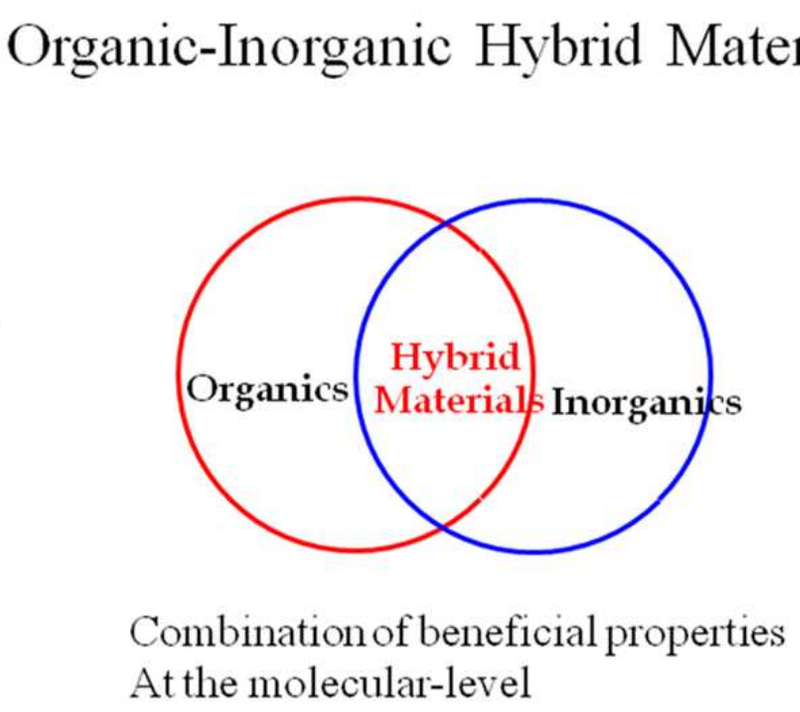

Figure 1. Organic/inorganic hybrid materials. [1]

In addition, a phase separation problem also limits to achieve a uniform mixing of multiple components during the bulk-mixing process.

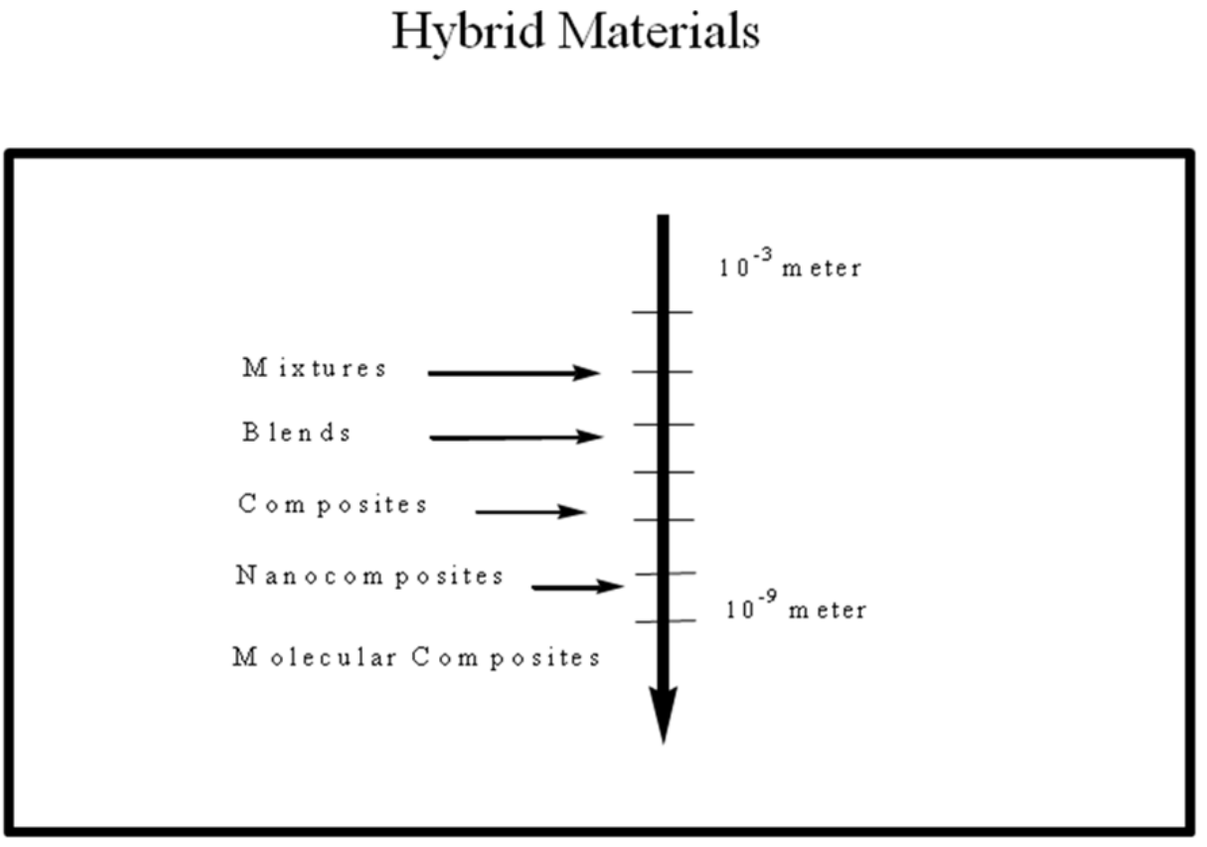

Figure 2. Relative size scale of mixing domains for different types of hybrid materials. [1-10]

To overcome those limitations of the bulk-scale mixing technique, *molecular-level hybridization technique* has been actively investigated. [1-10] This technique results in molecular-level composites, which are their domain sizes in the nanometer scale often create new properties, which would not be expected from those individuals by the loss of individuals' identities after the molecular-level mixing process thereby creating new properties.

Especially for optical device materials, desired properties of hybrid glasses can be chemically designed and then prepared by incorporating functional organic fragments between inorganic oxides.

With this strategy, novel optical device materials with beneficial properties can be obtained by embedding organic spacers into silicate network to create organically modified hybrid glasses as demonstrated in earlier publications (Figure 3). [1-10] Furthermore, the molecular-level mixing technique doesn't show any significant phase separation; because, *the molecular-level hybridization* is based on a microscopically homogeneous mixing and thus the uniform distribution of organic and inorganic moieties in a domain size at the molecular level is provided.

Those organically modified glasses mixed at the molecular scale, were provided by a molecular modification, which inserts desired organic fragments between two inorganic oxides to create entirely new optical properties. Figure 3 shows *the molecular-level hybridization* to produce polysilsesquioxanes.

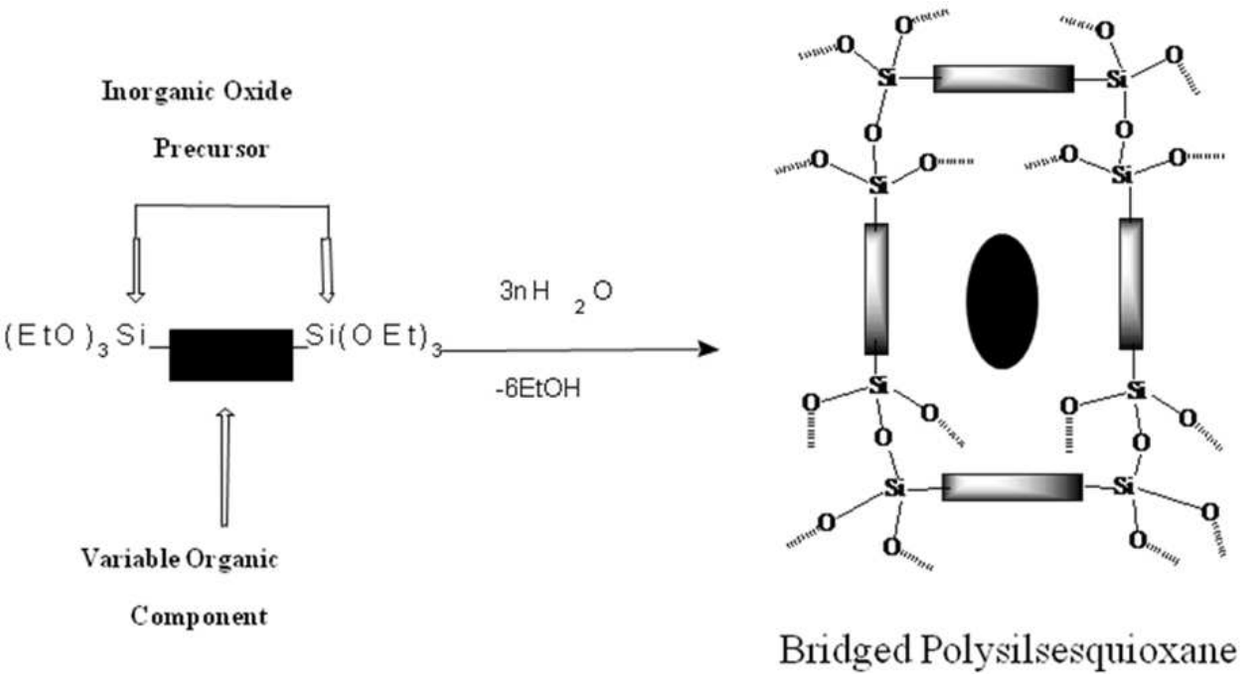

Figure 3. Molecular-level hybridization technique to produce polysilsesquioxanes. [6]

Bridged polysilsesquioxanes are a new family of molecular-level composites, which also a new version of hybrid glasses; these are prepared from hybrid sol–gel processable monomers through a sol-gel polymerization. These are microscopically homogeneous with uniform distribution of the organic spacers and thus also show an excellent optical transparency. There are many publications of novel optical device materials based on organic/inorganic hybrid glasses. [11-17]

In optical device materials, organically modified silicate glasses/transparent polymers have been actively pursued to develop novel optical devices, such as lasers, optical switches, optical fibers, waveguides, laser amplifiers, optical displays, and data storage devices.

[11-17]

In addition, we can also control the porosity of those organically modified silica, polysilsesquioxanes, by inserting different molecules or sizes of organic spacers as shown the void space in Figure 3 (right); due to the insertion of organic spacers, the porosity of the resulting hybrid glass significantly increased. [18-26]

The expanded pores allow us to dope semiconductor or metal particles without any significant mechanical cracks. *The molecular-level hybridization* also solves the phase separation problem during molecular-level mixing process.

The pore size of organically modified silicate materials can be controlled by both choices of organic spacers and sol-gel conditions. Those molecularly designed hybrid glasses have shown high surface areas and a relatively narrow distribution of pore sizes that range from the high micropore to the low mesopore domain (15-100 Å).

Several organic/inorganic hybrid sol-gel monomers have been molecularly designed and then synthesized for developing novel hybrid glasses. A variety of bridged polysilsesquioxanes, organically modified hybrid silica, have been designed by *the molecular-level hybridization* (Figure 4). [18-26]

Those functional organic spacers inserted in the silicate networks (Figures 3 and 4) can serve as dopant precursors to growth particles in the porous glassy hosts. Those void volumes in the glassy hosts can be a matrix for the growth of quantum dots, such as semiconductor or metal particles. No phase separation occurs during the corporations of those dopants.

In Figure 5, those sol-gel processable monomers contain functional groups, which are sol-gel polymerized under either acidic or base condition, and then produce highly porous xerogels. [4]

Due to the highly porous silicate matrices, we doped various dopants without any phase separation; for example, we prepared highly nano-porous polysilsesquioxane systems, and then controlled sol-gel conditions to dope nano-sized transition metal particles or semiconductor particles, such as CdS [18, 19, 21], chromium [20, 21], iron [22], cobalt [27], and platinum [28] into the silicate hosts.

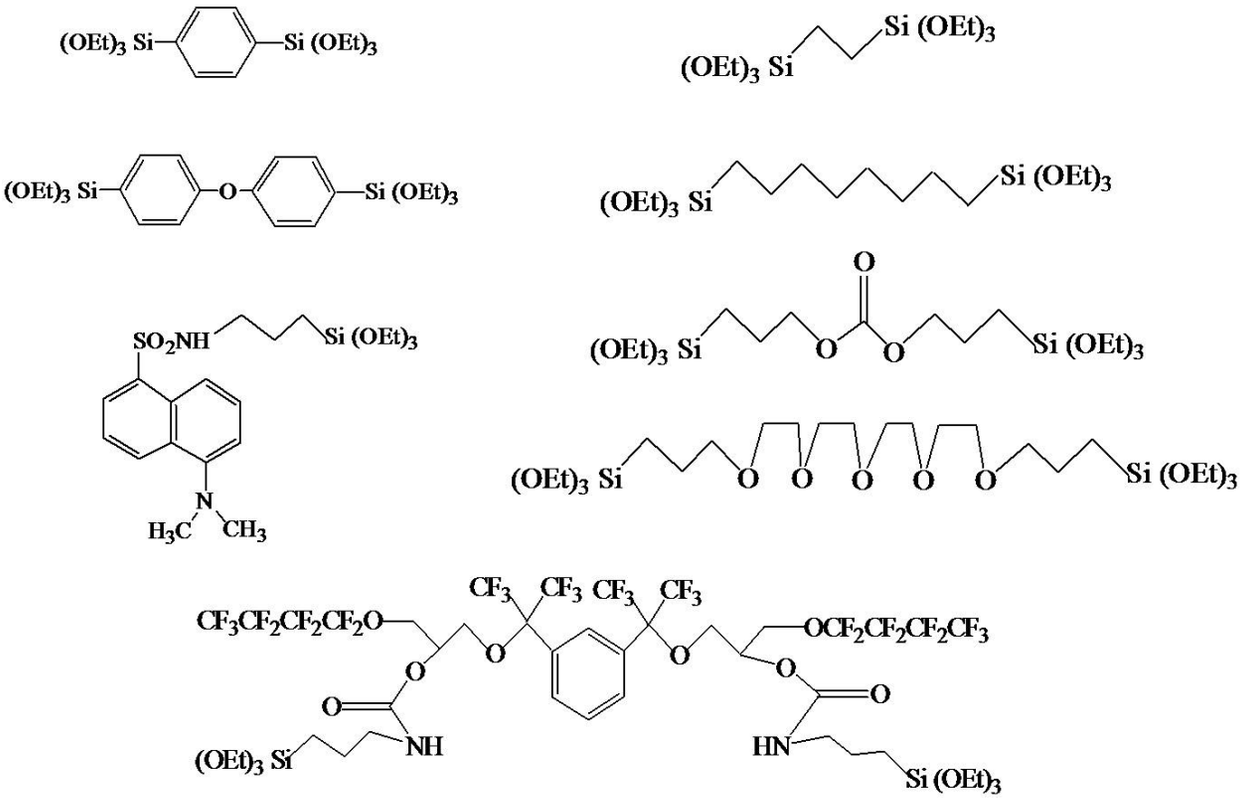

Figure 4. A variety of sol-gel processable monomers prepared by *the molecular-level hybridization*.

2. Novel optical device materials for laser amplifier [25]

We have developed novel laser devices based on those organic/inorganic hybrid glasses prepared by *the molecular-level hybridization.*

2.1. Rare-earth ion doped laser amplifier

Silicate-based optical fibers and planar waveguide amplifiers are widely studied for optoelectronic applications because of the superior chemical resistance and compatibility with other optical devices based on polymeric materials.

Transparent silica doped with rare-earth metal ions has been used for laser amplifiers, such as photonic fiber amplifiers, solid-state lasers, compact laser amplifiers, ultra short pulse lasers, high-power lasers, so on. [29-39]

Planar waveguides and fibers doped with rare-earth metal ions are a key challenge; thus, an enormous amount of publications in rare-earth metal ion doped optical devices has been found. [29-37] Fabrication of optical devices with high resolution offers an efficient approach to minimize the cost and size of optical amplifiers.

High gain laser amplifiers can be achieved by improving several relative factors, such as optical losses, phonon energies, pumping powers and distances, fluorescence life times, and refractive indices of optical medium. The lasing efficiency can be also improved by changing the chemical environment of rare-earth metal ions.

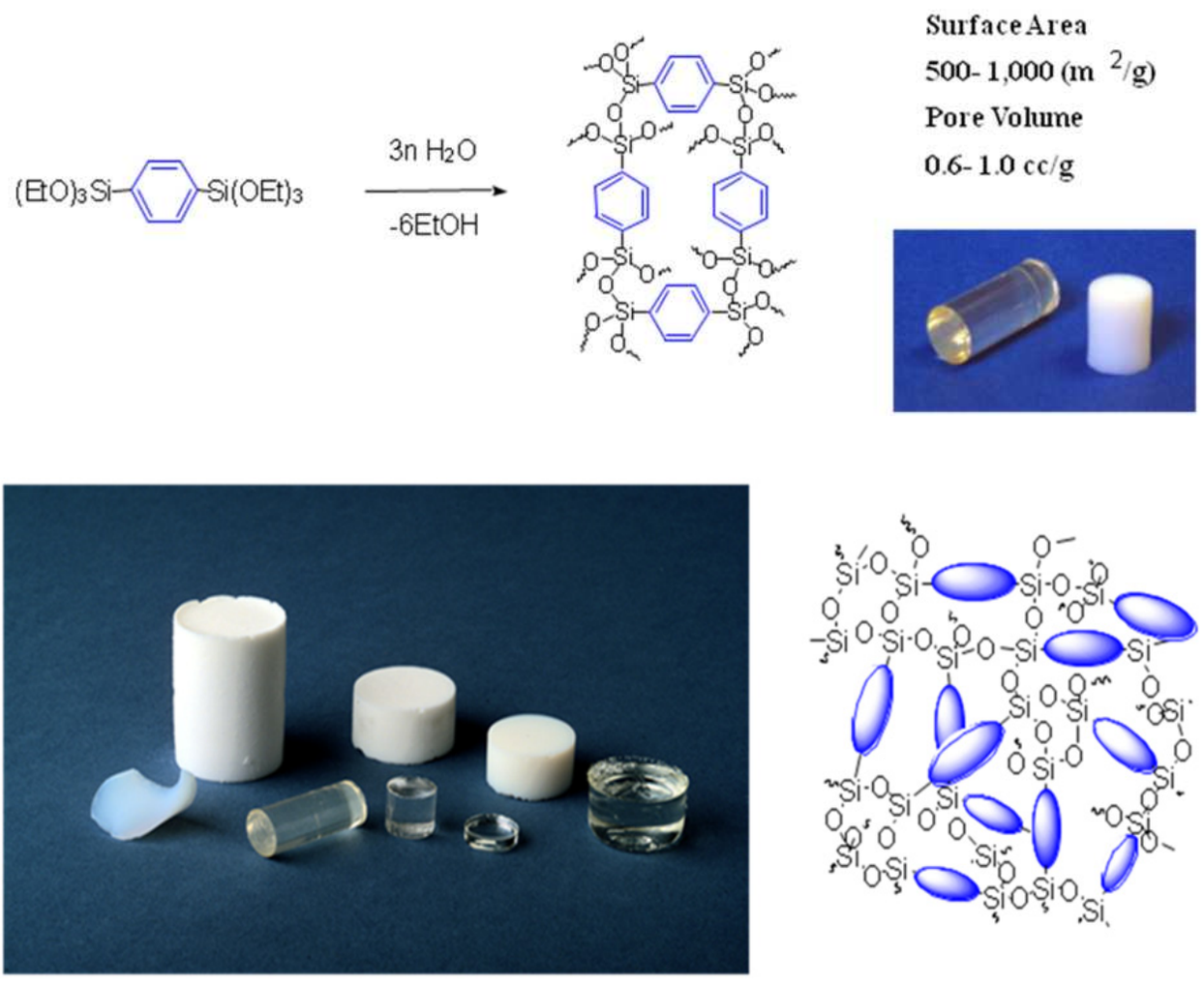

Figure 5. Highly porous polysilsesquioxanes. [4]

In a laser amplification based on rare-earth metal ions, erbium (Er) has been widely used as a gain medium due to its strong fluorescence at 1540 nm, which is a useful wavelength in optical amplifications. Especially, erbium-doped fiber amplifiers (EDFA) dominate this object of high gain optical amplifications. [32-35]

Since the performance of laser amplifiers is significantly influenced by optical media, scientists have been investigating organic/inorganic hybrid silicate hosts doped with Er^{3+} ions, in order to achieve high NIR efficiency and low phonon energy of the matrix to shorten the pumping distance and thus to obtain proper gain/life time. [32-35, 38, 39]

However, inorganic based optical media have shown a limitation to adjust the chemical environment of doped metal ions. For example, conventional silicate-based laser amplifiers often fail to produce high lasing performance because of a strong absorption raised from the OH-group at 1540 nm. The low concentration of erbium-ions in silicate host and the small absorption cross-section of the erbium-ions also limit the performance of normal silicate-based laser amplifiers since the doping level of rare-earth ions in glassy hosts significantly depends upon lasing efficiency.

Organic/inorganic hybrid glasses have been actively pursued as an alternative to conventional silicate glass for fabricating laser devices due to low temperature process and the promise of bringing new optical properties that are not possible from inorganic silica. [1, 40-42]

Furthermore, organic/inorganic hybrid silica is a good candidate to adjust the fluorescence environment of rare-earth metal ions by incorporating desired organic precursors into glassy hosts without any phase separation; usually, in inorganic silicate hosts, rare-earth ions tend to aggregate due to the absence of non-bridging oxygens, which cause a significant deduction of lasing efficiency. The synthesis of chemically modified silica with homogeneous doping of rare-earth ions is a key contributor to improve the performance of laser amplifications.

Optical device materials are required good optical transparency, controllable porosity, chemical purity, tunable refractive index, so on. Our goal for achieving those desired properties is to improve the fluorescence environment of Er^{3+} -ions in glassy hosts. For that, we devoted our attention to achieve an excellent chemical homogeneity of Er^{3+}-ion environment in glassy hosts.

2.2. Design of fluoroalkylene-bridged xerogel doped with Er $^{3+}$/CdSe

To demonstrate enhanced performance in laser amplifiers, we designed fluoroalkylene-bridged polysilsesquioxanes doped with Er^{3+}/CdSe nano-particles. [25] The fluoroalkylene-bridged silica was initially designed to reduce the phonon energy of the glassy host. Furthermore, CdSe nano-particles were also provided for further manipulation of the photochemical environment of erbium-ions in the matrix.

Use of organic silanes incorporates an organic fragment as an internal component of the silicate network. Sol–gel polymerization involves the hydrolysis of ethoxysilyl groups to yield silanols follows by subsequent condensation to form siloxane (Si–O–Si) linkages. In the sol-state, the condensation is insufficient to form a network, and the solution remains processable.

When sufficient cross-linking occurs, a network is formed and the transition from the sol-state to the gel state occurs. The presence of organic fragments within the 3-D structure imparts organic character to the hybrid glass that changes the microenvironment of additional fluorescence rare-earth ions incorporated in the glassy host.

In this study, fluorocarbon-linkages were designed to achieve high hydrophobicity within the hybrid glassy matrix. Erbium isopropoxide was also employed as the source for the Er^{3+} ions. Furthermore, CdSe nano-particles were also prepared and incorporated into the fluorinated glassy matrix to reduce the phonon energy of the glassy host (the phonon energy of CdSe = 200 cm^{-1}). [43]

In principle, when rare-earth metal ions are excited in transparent glassy matrices, they can behave as a laser, which enables amplification of the incident light intensity. The lasing performance significantly relies on rare-earth metal ion doping level, host materials' physicochemical property, and chemical homogeneity.

2.3. Experimental

A set of three different sol–gel processable monomers were prepared; tetraethoxy-silane (TEOS), 1,6-bis (triethoxysilyl)hexane, and 2,2,3,3,4,4,5,5-octafluoro-1,6-hexanediol bis(3-triethoxysilyl)propyl carbamate.

2.3.1. Tetraethoxysilane (TEOS)

TEOS was purified by drying over 4 Å molecular sieves followed by a vacuum distillation.

2.3.2. Synthesis of 1,6-bis(triethoxysilyl)hexane

1,6-Bis(triethoxysilyl)hexane was synthesized by a 'hydrosilylation' of the corresponding α, ω-alkyldienes with triethoxysilane employing chloroplatinic acid (H_2PtCl_6) as a catalyst. 1,5-Hexadiene (12.3 g, 0.15 mol), triethoxysilane (54.1 g, 0.33 mol), and chloroplatinic acid (1mL of 7.5×10^{-5} mol in isopropanol) were placed in a round bottle flask. After 10 hours of simple stirring process at a room temperature, the reaction mixture darkened.

The reaction was monitored by GC. The crude product was purified by a vacuum distillation with a resulting purity of 99.87 % by GC analysis: bp 130 ◦C/0.1 mmHg. The final product was verified by NMR analysis and mass spectroscopic analysis and was consistent with data previously report. [11]

2.3.3. Synthesis of 2,2,3,3,4,4,5,5-octafluoro-1,6-hexanediol bis(3-triethoxysilyl)propyl carbamate

2,2,3,3,4,4,5,5-Octafluoro-1,6-hexanediol (1g, 3.8 mmol) and 3-isocyanatopropyl triethoxy-silane (1.9 g, 4.3 mmol) were placed in a round bottom flask with a magnetic stirrer. The flask was sealed, purged with nitrogen, and 10 mg of dibutyl-tin-dilaurate was injected into the vial using a syringe as a catalyst.

The reaction was kept at room temperature under a nitrogen flow for several hours and monitored for the disappearance of the isocyanate peak at 2270 cm^{-1} (CN) in FT-IR. As the isocyanate group was converted to urethane group, identical peaks of 3400 cm^{-1} (NH) and 1720 cm^{-1} (CO) were observed. The product was dissolved in methanol and the tin catalyst was completely removed using a separated funnel. Methanol was then removed by a rotary evaporator. The product was used without further purification.

2.3.4. Er^{3+}-ion/CdSe doping procedure

A sol-gel processible monomer, erbium isopropoxide (Chemat Technology), was used as a source of Er^{3+}-ions. CdSe nano-particles were synthesized by a previously reported procedure. [44, 45] Those dopants were incorporated by mixing with the appropriate sol–gel mixtures (Table 1); xerogels-a5 and -a10 denote higher erbium concentrations (5 and 10 times higher) than that of xerogel-a system.

We also examined the homogeneity of three sol–gel mixtures (Figure 6). Ethanol was used as a solvent. A visual inspection was carried out to determine the comparative homogeneity of those sol–gel mixtures containing erbium isopropoxide (Figure 6-1) or both of erbium isopropoxide/CdSe nano-particles (Figure 6-2). In a mixing test (Figure 6), erbium isopropoxide was indicated as a bright pink color in the photographs. The CdSe nano-particles also show a characteristic bright orange-color in those mixtures.

Xerogels	Silicate matrices	Dopants
T-Xerogel	TEOS	None
H-Xerogel	Hexylene-	None
F-Xerogel	Fluoroalkylene-	None
Xerogel-a	TEOS	Erbium ions
Xerogel-b	TEOS	Erbium ions/CdSe
H-Xerogel-a	Hexylene-	Erbium ions
H-Xerogel-b	Hexylene-	Erbium ions/CdSe
F-Xerogels-a, -a5, and -a10	Fluoroalkylene-	Erbium ions
F-Xerogels-b, -b5, and -b10	Fluoroalkylene-	Erbium ions/CdSe

Table 1. List of xerogels doped with different components.

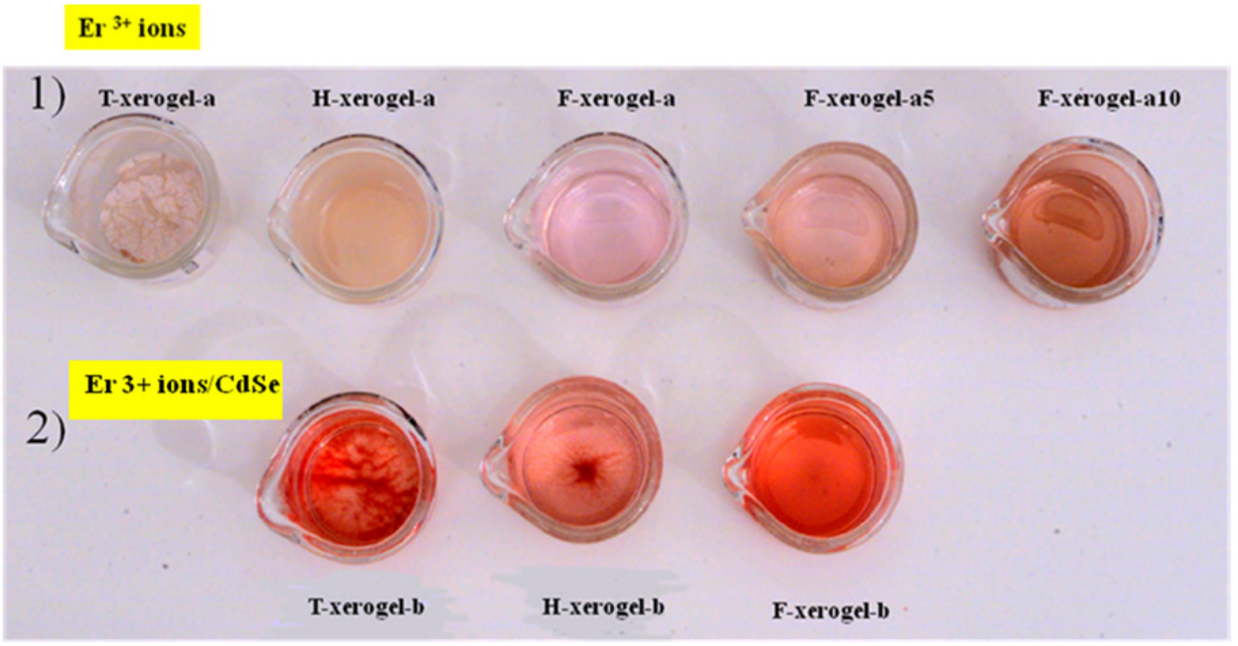

Figure 6. Mixing test.

2.3.5. Sol–gel procedures

Those sol–gel mixtures were then polymerized to produce the condensed xerogels under acidic condition using HCl as a sol-gel catalyst. Those xerogels were kept in a vacuum oven for 1–2 days to remove the remaining solvent and complete condensation.

2.3.6. Solid state NMR experiments

The ^{29}Si solid state NMR analysis of condensed xerogels was performed using a Varian Unity 400 solid state NMR spectrometer. The degree of condensation of undoped xerogels was computed from the single pulse magic angle spinning (SP/MAS) technique. A line fitting routine was also used in the analysis of the ^{29}Si NMR resonance in each spectrum to establish the siloxane ratio in the different structures.

2.3.7. Fluorescence measurements

Fluorescence study of Er^{3+}-ions doped into those glassy matrices was carried out by using the Ar+ ion laser (488 nm). Laser power densities ranging from 1.5 to 3 Wcm^{-2} were used for the measurements.

2.4. Results and discussions

2.4.1. Mixing test

During the mixing test (Figure 6), we observed that the TEOS-based mixtures revealed a substantial degree of undesirable phase separations after doping with the Er^{+3}-ion sources or Er^{+3}/CdSe nano-particles. For example, in Figure 6-1, the T-xerogel-a mixture shows a significant phase separation even at the lower erbium concentration.

In contrast, hybrid sol–gel monomer mixtures showed significantly less phase separations (Figure 6). Hybrid sol–gel monomer mixtures accommodate and homogeneously distribute the Er^{3+}/CdSe source without any significant phase separation. In mixing test with hybrid sol-gel monomer mixtures, we observed no momentous phase separation, especially in the highly fluorinated sol-gel mixtures.

It is apparent that the TEOS-based sol–gel mixture has a rather limited solubility of erbium-ions, and hence a limited capability for fluorescence enhancement.

Subsequently, we provided CdSe nano-particles by following the earlier method [44, 45], and then added CdSe nano-particles into those sol–gel monomer mixtures containing the the Er^{3+}/CdSe source. Usually, CdSe nano-particles synthesized in colloidal configuration are suitable for incorporation into a variety of hosts including sol–gel mixtures. The comparative homogeneity of the three sol-gel monomer mixtures containing both of the erbium isopropoxide and CdSe nano-particles is also shown in Figure 6-2.

In Figure 6-2, TEOS-based mixture (T-xerogel-b) shows the CdSe nano-particles segregated in the mixture; the orange-colored CdSe nano-particles are observed to phase separate within the mixture.

In contrast, a hybrid sol-gel monomer system (H-xerogel-b) shown in Figure 6-2, the CdSe nano-particles mixed better than the T-xerogel-b. In the H-xerogel-b mixture, most of CdSe particles were dissolved, except some of undissolved orange-colored CdSe residues toward the middle of the container. In fluorinated mixture (F-xerogel-b) shown in Figure 6-2, CdSe nano-particles were incorporated without phase separation. This result demonstrates that the fluoroalkelene-bridged sol-gel monomer has the capability of uniformly incorporating both types of dopants without any phase separation.

2.4.2. Solid state NMR analysis

The chemical composition and the degree of condensation for those condensed xerogels can be determined by solid state nuclear magnetic resonance, infrared, and Raman spectroscopies. [1]

We employed a solid state NMR analysis to determine the degree of condensation of hybrid glassy hosts. ^{29}Si solid state NMR was used to identify the Si–O–Si bonds in variety states of condensation for three matrices. Single pulse magic angle spinning NMR methods were employed for the characterization of T-xerogel, H-xerogel, and F-xerogel to calculate the degree of condensation.

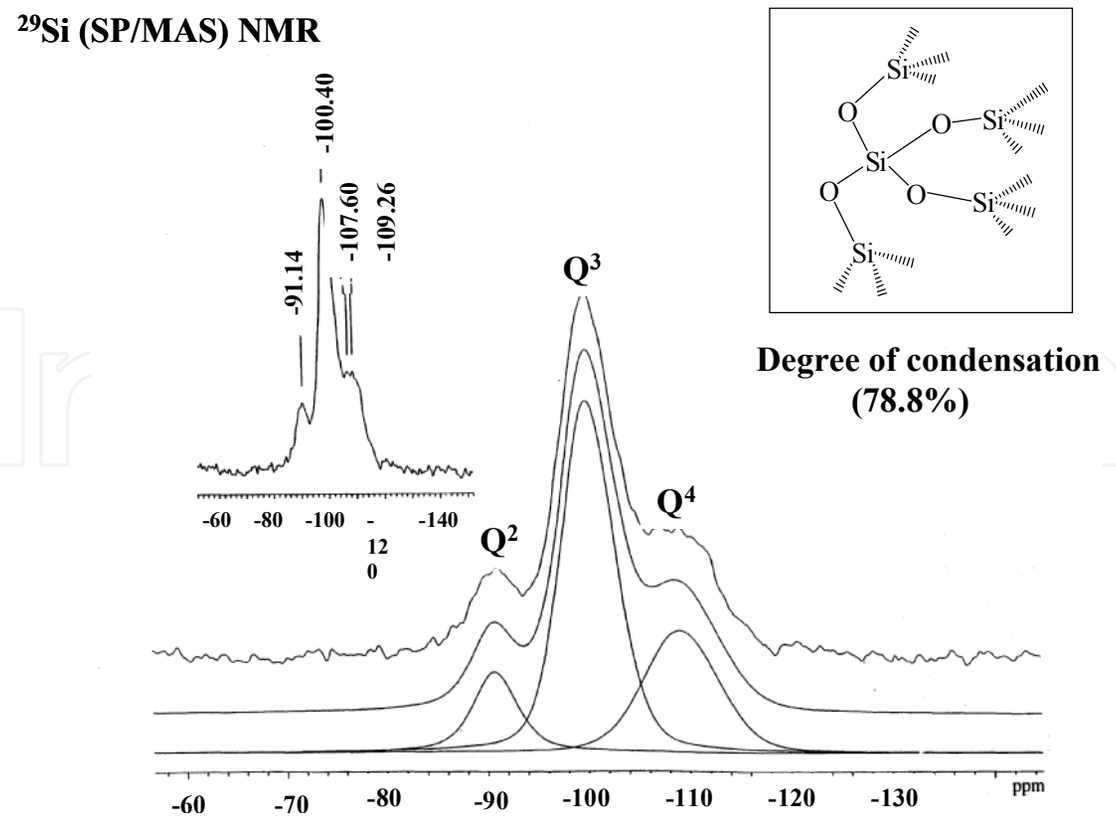

Figure 7. ^{29} Si solid state NMR spectrum for undoped T-xerogel.

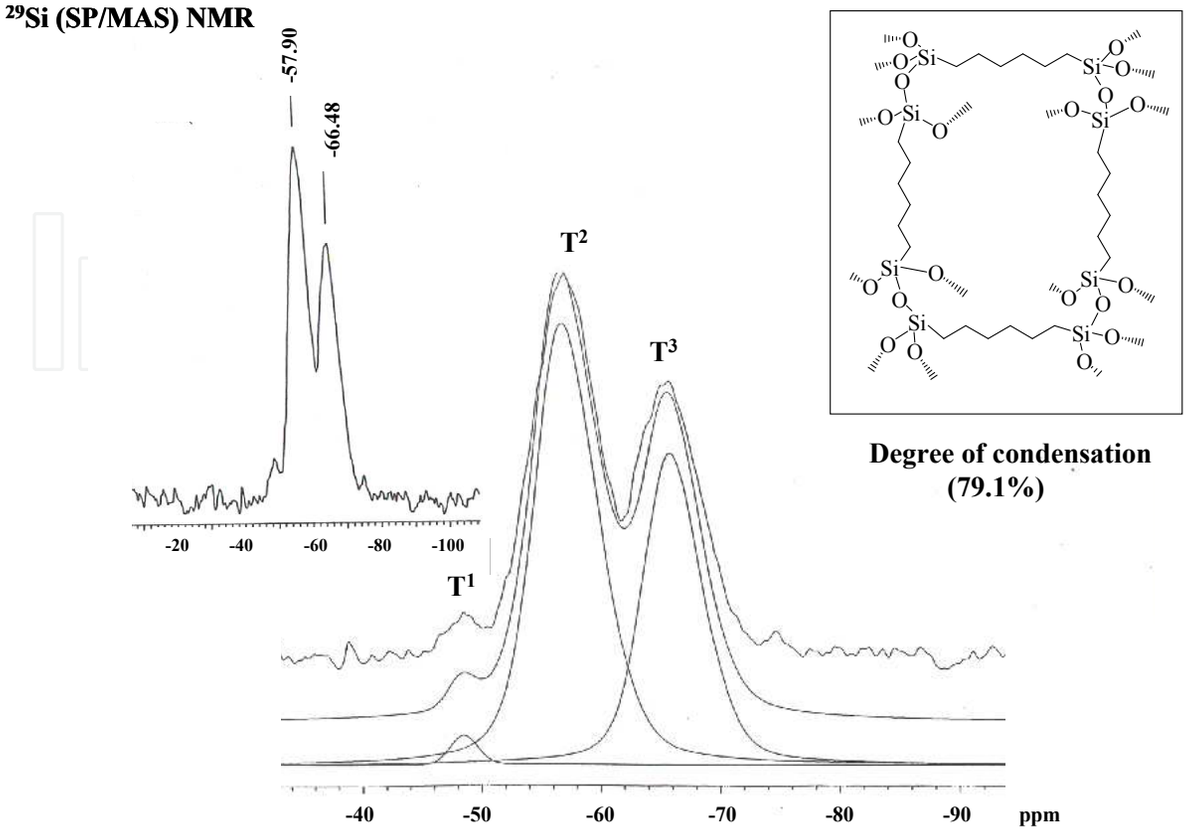

Figure 8. [29] Si solid state NMR spectrum for undoped H-xerogel.

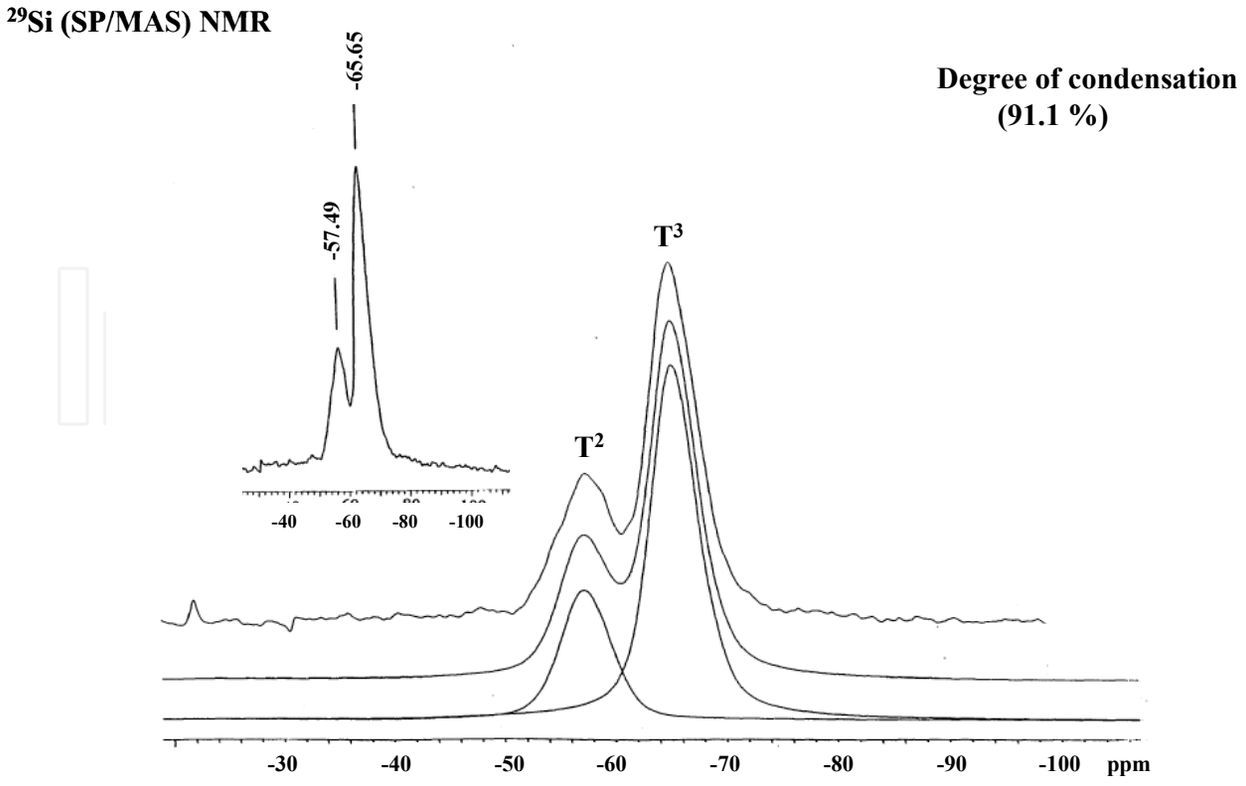

Figure 9. [29] Si solid state NMR spectrum for undoped F-xerogel.

Figures 7-9 show the result of ^{29}Si SP/MAS solid state NMR analyses and peak deconvolution lines of both normal and modified silicate systems.

Figure 7 shows the ^{29}Si SP/MAS solid state NMR spectrum of the undoped T-xerogel. As shown in Figure 7, it reveals three peaks, which correspond to the Q^2, Q^3, and Q^4. The degree of condensation for the T-xerogel was calculated to be 78.8%.

Figure 8 shows the ^{29}Si SP/MAS solid state NMR spectrum of the undoped H-xerogel. Three peaks shown in spectrum correspond to the T^1, T^2, and T^3. The degree of condensation of the H-xerogel was also computed to be 79.1%.

The ^{29}Si SP/MAS solid state NMR spectrum of the undoped F-xerogel is given in Figure 9. The T^1 peak is not observed in this system. Also, the T^3 peak intensity in Figure 9 is higher than that of T^2. We found that the degree of condensation was dramatically increased to 91.1% in this case.

The high degree of condensation in the undoped F-xerogel can be explained as a result of the electron-withdrawing effect of the fluorine, which causes a partial positive charge at the silicon facilitating nucleophilic attack in the sol–gel process thus accelerating hydrolysis and condensation.

The high degree of condensation, disappearance of T^1 peak, and enhanced T^3 peak in the F-xerogel indicate a low level of hydroxyl group content and a greater degree of condensation when fluorinated alkylene groups are present in the glassy hosts.

Si–OH groups show a high phonon energy (3000–3500 cm^{-1}) at 1540 nm. [43]

The reduction in hydroxyl content in the F-xerogel matrix decreases the phonon energy of the matrix. The exclusion of moisture from the high hydrophobicity of the fluoro-alkylene groups in the F-xerogel matrix may also contribute to reduce the absorption at 1540 nm with a concomitant increase the fluorescence intensity of Er^{3+}-ions.

All these effects contribute to the increased fluorescence from erbium-ions in the fluorinated hybrid glassy matrix.

2.4.3. XPS analysis

We also employed a XPS study to determine the chemical composition of F-xerogel-a. [46]

A full XPS scan was obtained in the 0–1100 eV range. Detail scan was also recorded for the Er (4d) region. Figure 10 shows a full spectrum for F-xerogel-a. The XPS spectrum of F-xerogel-a shows an erbium peak at ~169 eV, which corresponds to the presence of Er_2O_3.

The atomic compositions were evaluated in this study. The concentration of each element (atomic %) was calculated; O(1s)—22.74 atomic %, C(1s)—53.29 atomic %, Er(4d)—1.49 atomic %, F(1s)—9.02 atomic %, Si(2p)—10.91 atomic %, N(1s)—2.55 atomic %. From the XPS analysis, it was estimated that the F-xerogel-a contains ~1.49 atomic % of erbium.

2.4.4. Fluorescence measurements

Erbium-ions incorporated into glassy matrices exhibit well defined energy level transitions in 4f-shell electronic configurations.

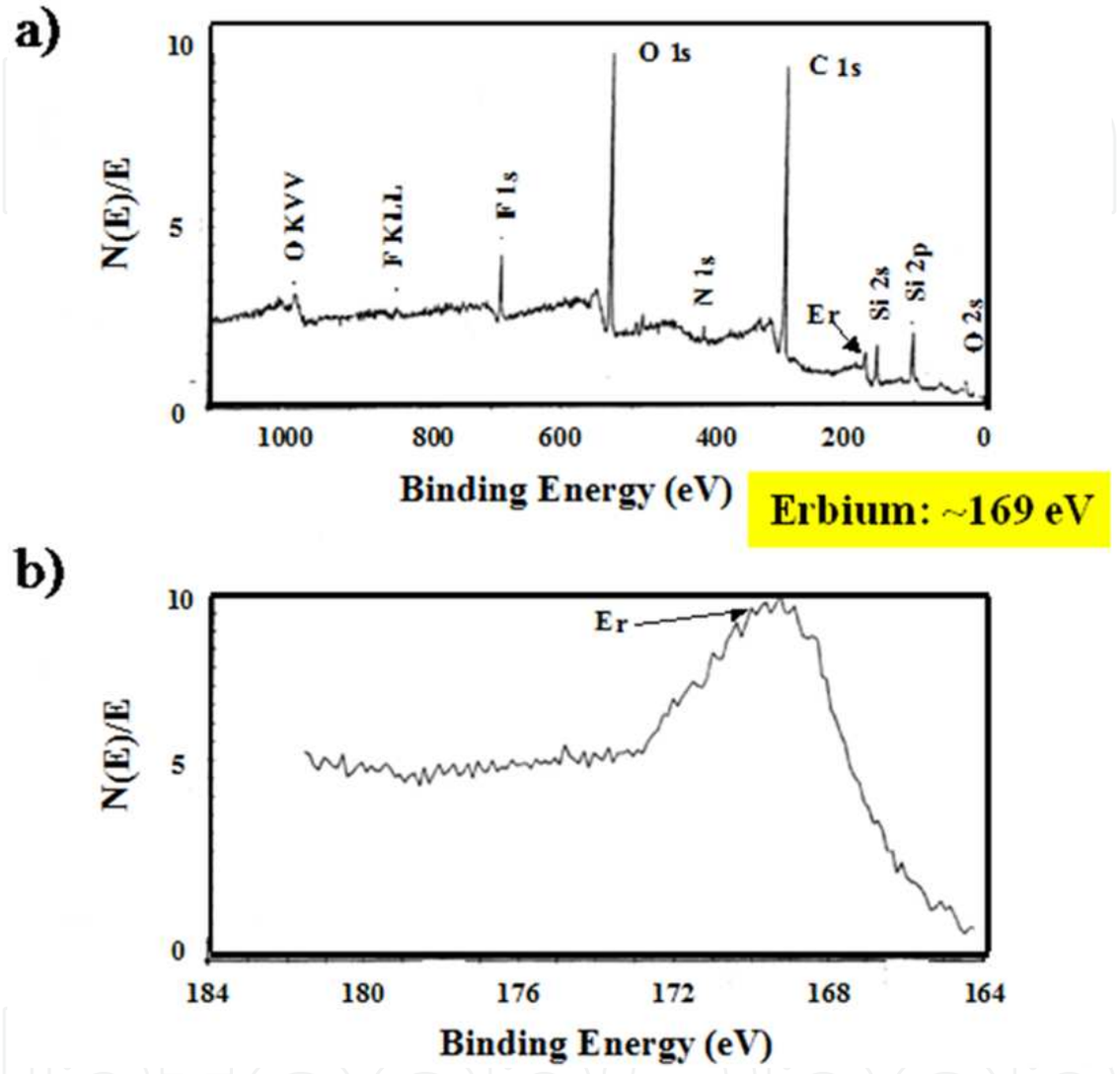

Figure 10. XPS Analysis of F-xerogel-a.

For erbium-ions, the $4I_{13/2}$ to $4I_{15/2}$ transition is important in optical communications; because, it results in fluorescence at 1540 nm, which is the most important wavelength regime for optical communication applications, especially in long-distance telecommunication networks. [47]

We examined how the fluorescence intensity of erbium-ions was dependent upon the matrix environment when fluorine and CdSe nano-particles were incorporated into hybrid glassy hosts. We carried out fluorescence analysis of erbium-ions around 1540 nm. The results are shown in Figures 11-13.

A comparison of fluorescence intensities from erbium-ions doped into different glassy hosts is shown in Figure 11 (H-xerogel-a and F-xerogel-a).

In Figure 11, fluorescence intensity of erbium-ions increased significantly more in F-xerogel-a than the other hybrid system of H-xerogel-a.

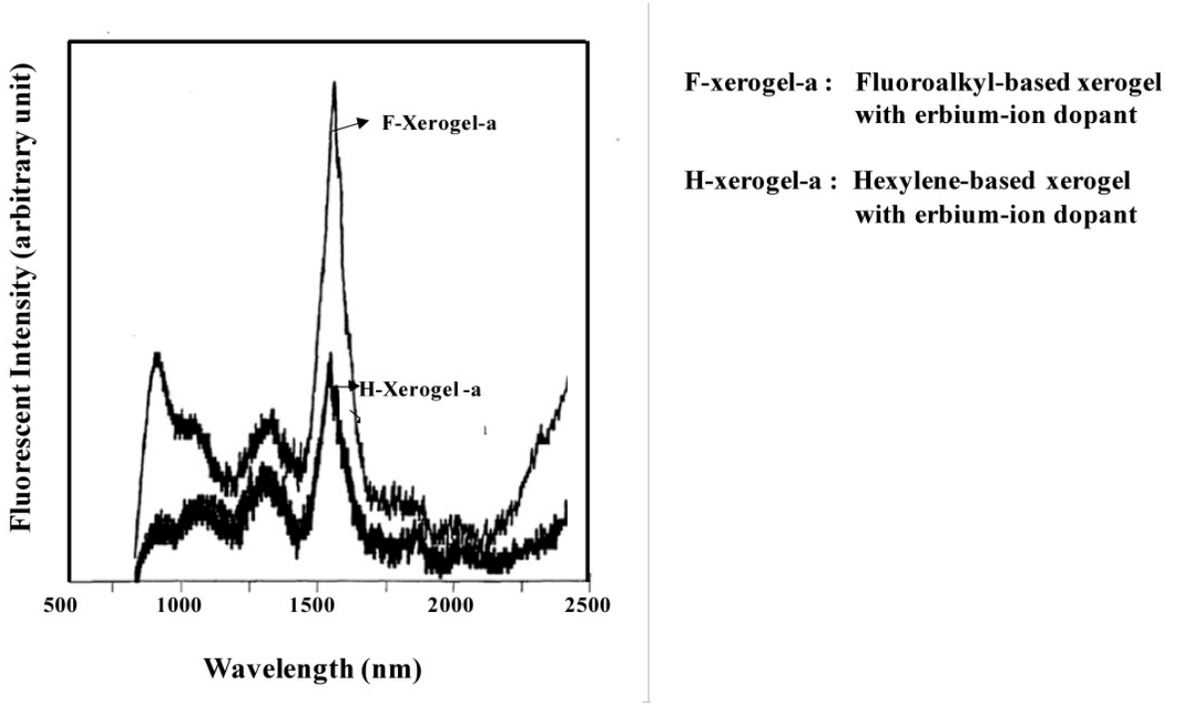

Figure 11. Photoluminescence of erbium-ions; different silicate matrices. Comparative fluorescence intensities of two different hybrid xerogels doped with Er^{+3} ions using a low power of 1.5 Wcm^{-2}.

The explanation of Figure 11 is that the enhanced fluorescence intensity of the fluorinated matrix is attributed to mainly its high hydrophobicity combined with the lower OH-group contents, which revealed in NMR study in Figure 9. Solid state silicon NMR analysis indicates an enhanced condensation in fluorinated xerogel compared to that of alkylene-bridged xerogel. The fluorinated hosts also showed an excellent chemical homogeneity in mixing test (Figure 6), which significantly affects the lasing performance.

Further investigations in fluorescence studies have been carried out. Since it is important to consider the erbium-ion concentration effect, fluoroalkylene-based glasses doped with two different levels of erbium concentrations were prepared for the determination of erbium-concentration effect (Figure 12).

Intensity of those xerogels (F-xerogel-a and F-xerogel-a5) was measured at a power density of 3 Wcm^{-2}. As shown in Figure 12, the fluorescence intensity increases (the upper curve) in the case of F-xerogel-a. It can be explained that the higher erbium concentration of F-xerogel-a5 caused a low lasing efficiency due to the "self-quenching effect."

Fluoroalkylene-bridged xerogel containing Er^{3+}-ions shows significantly reduced absorptions at the 1540 nm by reducing amounts of uncondensed hydroxyl groups.

The presence of CdSe nano-particles also significantly influences the fluorescence environment of Er^{3+}-ions in different glassy hosts, resulting in the increased fluorescence intensity. [43]

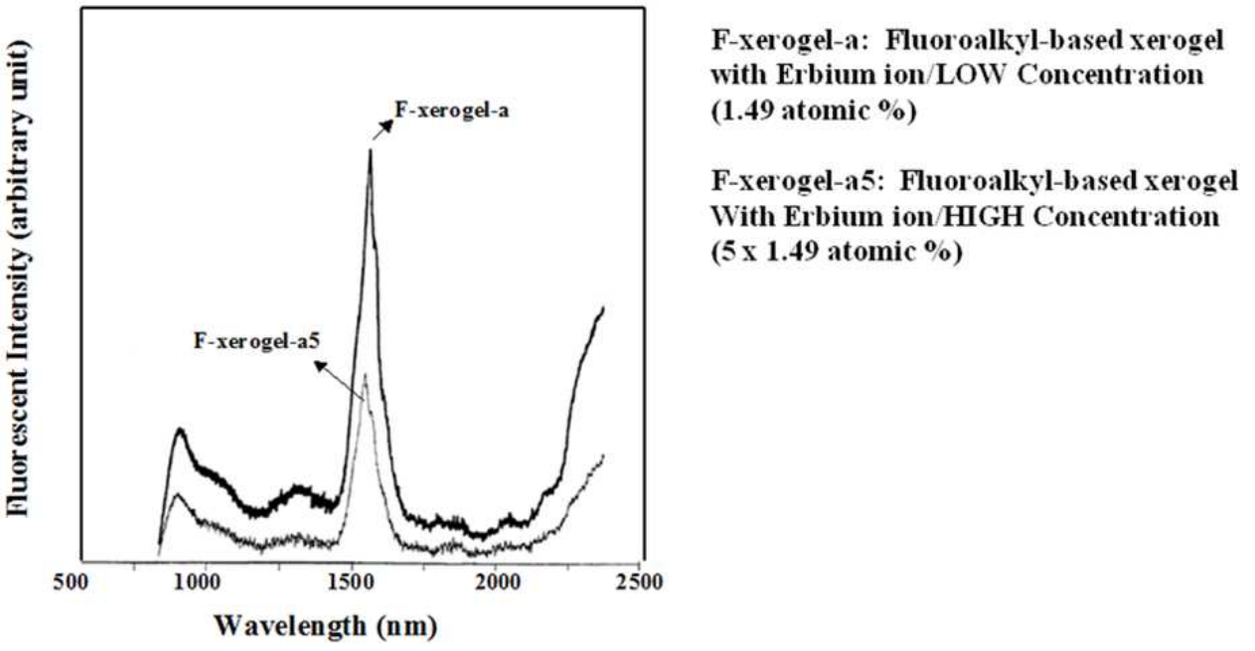

Figure 12. Photoluminescence of erbium-ions; different erbium concentrations. Comparative fluorescence intensities of xerogels with different Er^{3+}-ion concentrations (F-xerogels-a and -a5) using a power of 3.0 Wcm^{-2}.

CdSe nano-particles were used to modify the photochemical environments of erbium-ions in glassy hosts by taking advantage of a low phonon energy of CdSe phase (200 cm^{-1}) [43], since the incorporation of semiconductor nano-particles resulted in an enhancement of the semiconductor-to-erbium transfer when the quantum well and erbium-ion transition energies became close.

We thus examined the fluorescence of erbium-ions surrounded by CdSe nano-particles since it was anticipated that the presence of CdSe in the modified glassy hosts would affect the fluorescence performance (Figure 13). In order to test this, we prepared fluoroalkylene-bridged hybrid glasses doped without and with the CdSe nano-particles, F-xerogels-a5 and F-xerogel-b5, respectively.

As shown in Figure 13, the fluorescence intensity of F-xerogel-b5 is dramatically increased, which indicates an improvement in lasing efficiency by modifying photochemical environments of erbium-ions.

By taking advantage of the structural features and uniform doping capability in modified glassy matrices, we successfully demonstrate that the fluorescence environments of erbium-ions can be a key to improving the performances of optical devices like laser amplifiers to overcome the limitations in inorganic silica.

In conclusion, we have demonstrated here a promising result in laser amplifications by employing bridged polysilsesquioxanes doped with Er^{3+}-ions/CdSe nanoparticles.

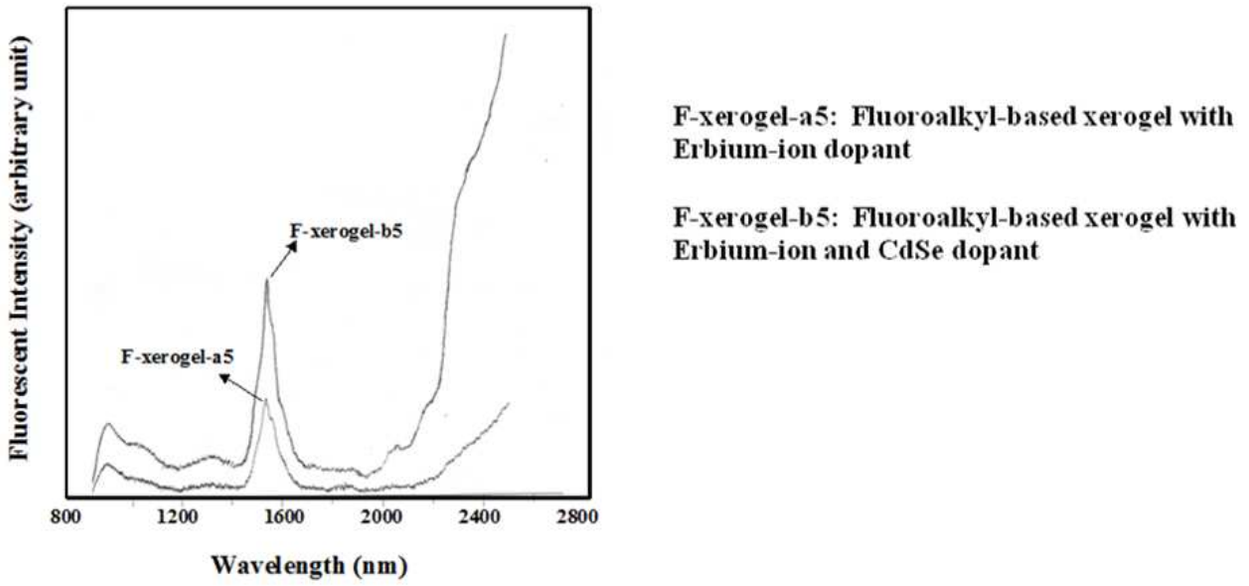

Figure 13. Photoluminescence of erbium-ions; CdSe nanoparticle effect. Comparative fluorescence intensities of fluoroalkylene-bridged xerogels doped without and with the CdSe nano-particles (F-xerogels-a5 and -b5), respectively, using a high power of $3Wcm^{-2}$.

To avoid the high phonon energy raised from OH-groups (3000–5300 cm^{-1}) at 1540 nm [43], we designed highly fluorinated hybrid glasses to shorten the fluorescence-level life times of dopants, which adversely affect optical device performance.

The presence of CdSe nano-particles, by virtue of its lowering of phonon energy, also appears to significantly influence the nature of the surrounding photochemical environment of Er^{3+}-ions in the fluorescence study.

From those study, we found that the control of such optical materials' properties affect the performance of optical devices via molecular tailoring strategy, which is molecular-level hybridization technique.

3. Novel optical device materials for acoustic wave [26]

3.1. Novel optical device materials based on polysilsesquioxanes

The preparation of semiconductors, metals, and ions in a variety of transparent materials has been actively pursued for optical devices. Scientists have taken a great attention to incorporate metal particles/ions in glassy hosts to develop high performance optical devices.

Chemists also have taken intensive challenges on how to achieve homogeneous incorporations of semiconductors or metal particles in glassy hosts, which are significantly influenced by diffusion of reagents, the number of nucleation sites, stabilization of growing particles by surface functionality, the boundary constraints of the growth matrix, and the opportunity for equilibration or "ripening" of particles formed under kinetic growth conditions. [2, 21, 48, 49]

Organically modified hybrid glasses, which were prepared by '*molecular-level hybridization*' (Figure 3), are a good candidate to develop laser device materials due to their easy processability and chemical modification.

Polysilsesquioxanes can be prepared by '*molecular-level hybridization'*, which inserts different types and sizes of organic spacers between two inorganic oxides. The sol-gel chemistry was employed to covalently incorporate semiconductors/metals in various oxidation states as an integral component of hybrid silicate matrices.

The 'molecular-level corporation techniques' also can be employed for the incorporation of semiconductors or transition metals/ions dispersed in optically transparent silica to prepare novel optical devices.

Especially, polysilsesquioxanes are microscopically homogeneous due to uniform distribution of organic and inorganic moieties in a domain size at the molecular level. Hence, these hybrid glasses can be used for optical device materials since the molecular-scale mixing process significantly reduces phase separation and thus produces high quality of optical clearance.

In this work, we molecularly designed a novel hybrid glass to develop alkylene-bridged polysilsesquioxanes doped with Cr^{o}/CrOx phases (Figure 14). The doped xerogel film effectively generates a HUGE ACOUSTIC WAVE.

3.2. Periodic alignment of alkylene-spacers to create molecular-scale optical grating for acoustic wave

Usually, scientists prepare 'periodic metal frames' to create 'diffraction grating' at the bulk-scales. For example, in a spectroscopic monochromator, 'optical grating effect' is used to split, and then diffract the light into several beams traveling in different directions.

In 'grating equation', the directions of these beams rely on the spacing/distances of the grating, which has a periodic structure of the media, and the wavelength of the light. Gratings, which modulate the phase rather than the amplitude of the incident light, can be also produced. A key idea of the periodic alignment of alkylene-spacers is to create 'a molecular-scale diffraction grating effect' and thus to generate a huge acoustic wave.

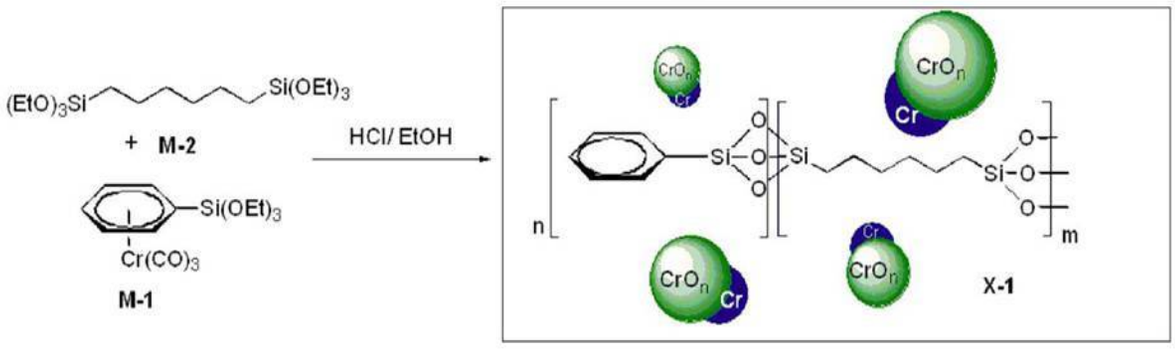

Figure 14. Hexylene-bridged polysilsesquioxane doped with Cr^{o}/CrOx.

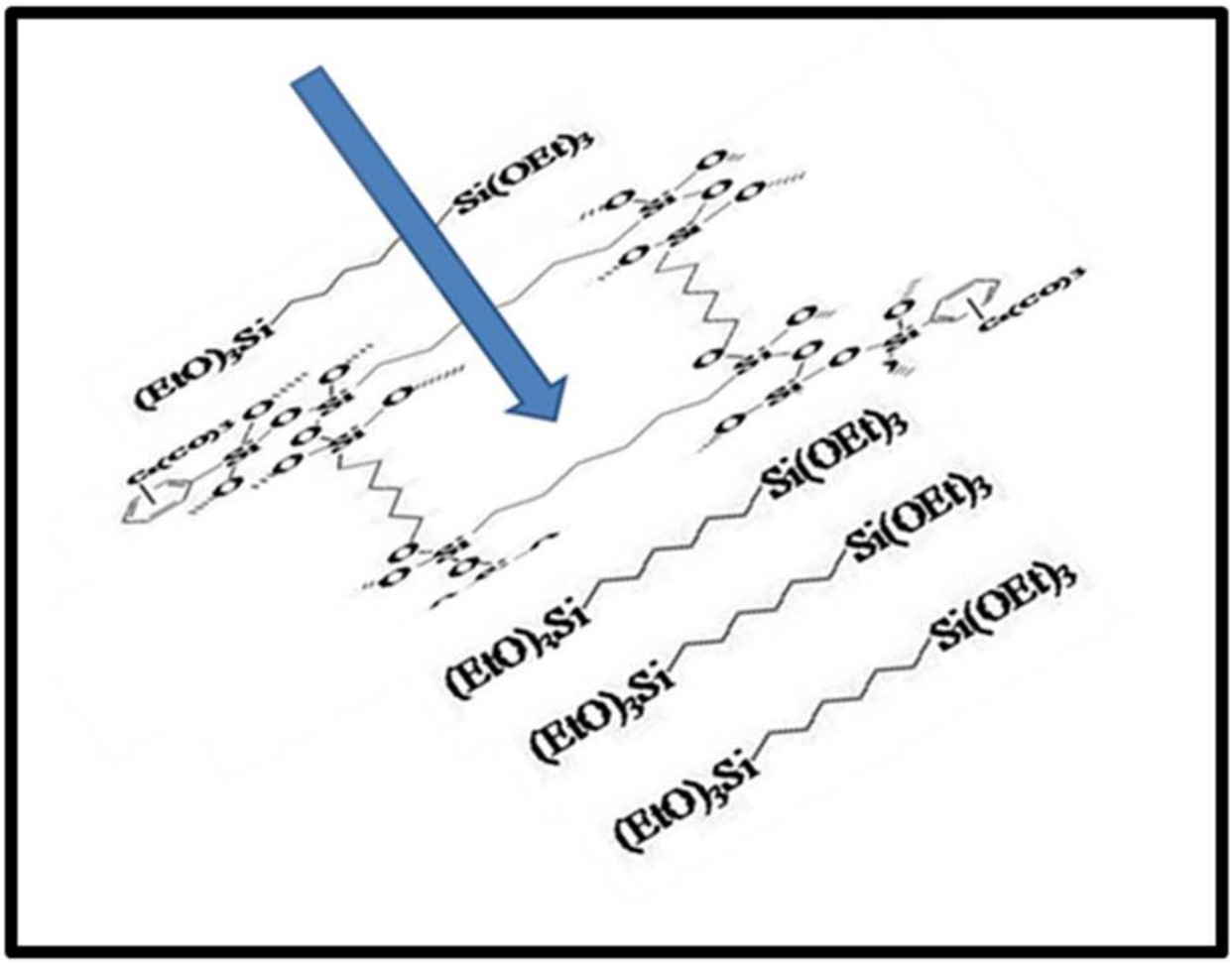

Figure 15. Periodic alignment of alkyl-chains to create "optical grating" at the molecular scales.

Figure 15 illustrates a light that passes through 'optical grating at the molecular-scales' designed in the hybrid silicate host. As you can see, the periodic alkylene-spacers create 'effective diffraction grating at the molecular scales' and thus produces a huge acoustic wave. This is a new optical phenomenon, which hitherto hasn't been discovered.

In addition, the distance between those alkyl-spacers can be also "controlled" by both choices of different organic spacers and sizes of sol-gel monomers. This is an effective method of developing new laser device materials based on organically modified silica, polysilsesquioxanes.

Usually, when the laser beam goes through a solid medium, the density wave is linear; because, in solid media, heat doesn't decay through the solid medium effectively.

Interestingly, the highly compressed xerogel, hexylene-bridged polysilsesquioxane doped with Cr^{o}/CrOx phases showed a strong 'acoustic response' as much as a liquid.

In our laser experiments, we calculated physical parameters of hexylene-bridged xerogel doped with Cr^{o}/CrOx phases. The coefficient of phonon diffraction (D) of the doped xerogel was FIVE times smaller than that of normal glass. Which means that the thermal conductivity of the doped xerogel, is FIVE times less than that of normal glass.

In addition, the diffraction efficiency, absorption light efficiency, (45%) of the doped xerogel is higher than that of methanol (25%), which means the COMPRESSIBILITY of the doped xerogel is as effective as liquid. The acoustic refractive intensity and acoustic response generated from the doped xerogel was as strong as liquid. Therefore, the doped xerogel serves as a 'heat generator,' and thus the heat gets transferred into expansion or compression wave (acoustic waves) effectively.

There were a lot of efforts to develop novel laser device materials based on organic and inorganic hybrid silica. [50-54] Especially, this is a unique approach to create an effective optical grating, which brings a HUGE ACOUSTIC RESPONSE by setting up a molecular-scale optical grating effect. By building up the periodic structure of long alkyl-chains in the hybrid glassy hosts, we obtained a HUGE ACOUSTIC WAVE, which hasn't been found. This is a new optical phenomenon.

3.3. Novel sol-gel condition to produce thin films of alkylene-bridged xerogel doped with Cr^{o}/CrOx

The new optical property partially rose from a new sol-gel mixing condition, which effectively produces HIGHLY COMPRESSED, THIN xerogel films. Conventional sol-gel conditions often result in poor optical transparency/mechanical property. For example, xerogels obtained from the conventional sol-gel conditions are thick and brittle materials. Those thick xerogels are difficult to handle, especially for optical applications.

The limitation motivated us to find a novel sol-gel mixing condition, which produces a highly compressed, thin sol-gel film with a smooth surface and excellent optical clarity.

We discovered a novel sol-gel mixing condition, which results in such a thin xerogel film of alkylene-bridged polysilsesquioxanes doped with Cr^{o}/CrOx with a low thermal conductivity and high compressibility (Figure 16). [26]

During the sol-gel polymerization, a volume of the sol-gel mixture was dramatically reduced, and then left a green sol-gel film with an excellent optical clarity (Figure 16).

For a source of chromium, we have synthesized a sol-gel processable chromium precursor [20, 26]; we prepared a green sol-gel film based on hexylene-bridged polysilsesquioxanes doped with Cr^{o}/CrOx phases using the chromium precursor. [20, 26]

In Figure 16 (top left), it shows a undoped hexylene-bridged polysilsesquioxane prepared from our novel sol-gel mixing condition; it was plastic-like a xerogel monolith. As you see in Figure 16 (top, left), it shows an excellent optical transparency.

Doped xerogels were also prepared in Figure 16 (top, Right and bottom). Those green xerogels were obtained as "plastic-like thin films" with an excellent optical compressibility and low thermal conductivity. It was prepared without any mechanical damage/cracking problem.

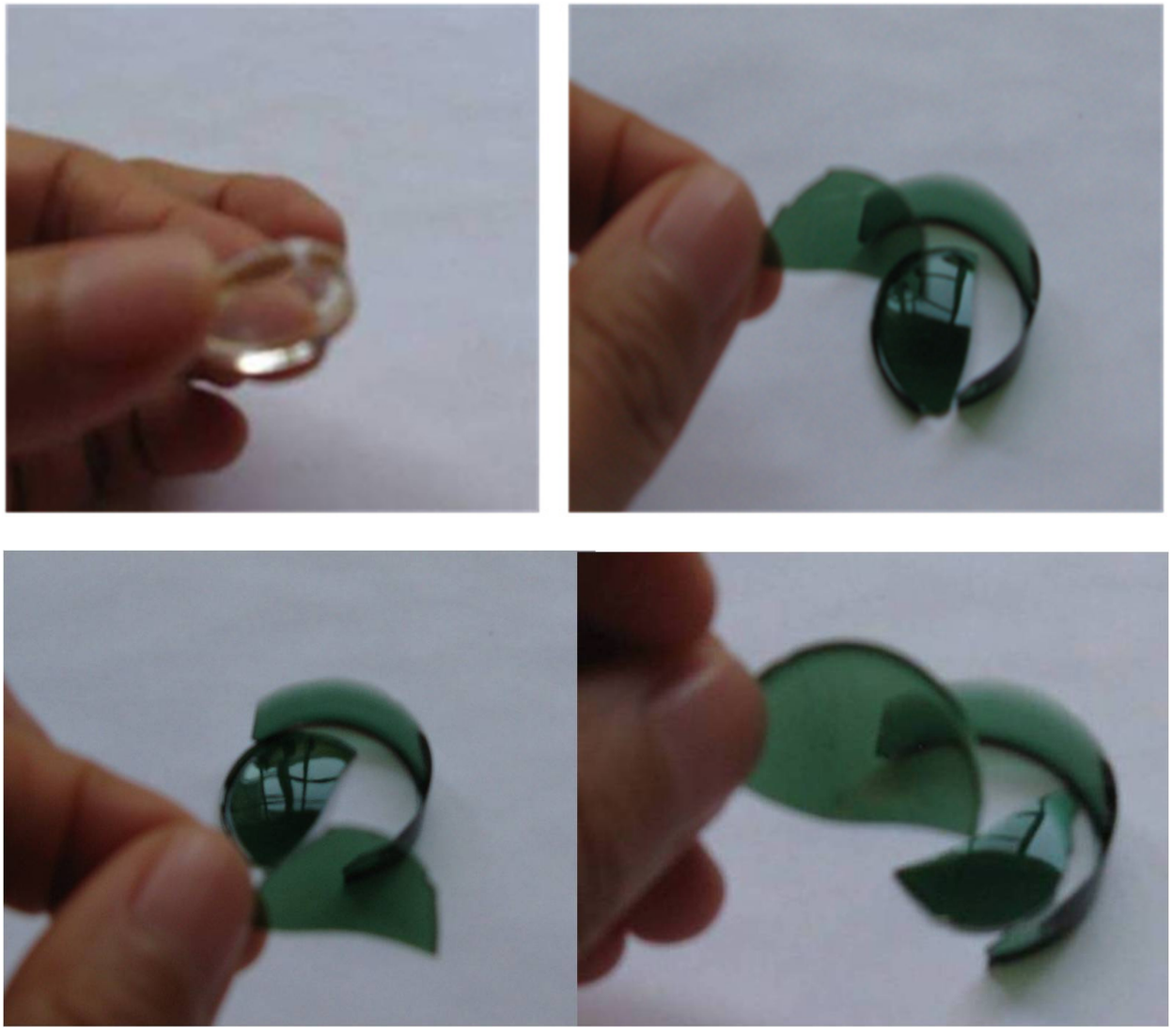

Figure 16. A comparative photos of undoped- (top left) and the Cr^{o}/CrOx doped- (top right and bottom) xerogels based on hexylene-bridged polysilsesquioxane under an acidic condition.

3.4. Experiments

3.4.1. Preparation of doped xerogels

Syntheses of sol-gel monomers, 1,6-bis(triethoxsilyl)hexane and chromium precursor, η^6-chromium tricarbonyl(triethoxysilyl)benzene, were carried out by following the earlier procedures, respectively. [11, 20]

Subsequently, hexylene-bridged xerogel doped with Cr^{o}/CrOx phases was prepared by a copolymerization of η^6-chromium tri-carbonyl(triethoxysilyl)benzene and 1,6-bis(triethoxsilyl)hexane under an acidic condition (Figure 17). A green glass was provided after the sol-gel polymerization (Figure 16).

Density of the doped xerogel was measured to be 1.2696 g/cm^3 using a He-gas pycnometer. From AAS analysis, the chromium amount was also analyzed to be 1.4% by weight.

3.4.2. TEM, EDAX, and electron diffraction analysis

A novel periodic alignment of alkylene-spacers in hybrid glass was specifically designed for creating 'a molecular-scale diffraction grating.' We employed TEM analysis to identify the molecular alignment built up in the hybrid silicate matrix.

The doped hybrid glass under an acidic condition (Figure 17) was ground to powders with a particle size (<150 μm), and deposited on a plasma-etched carbon substrate supported copper grid. TEM dark-field images were obtained using a Philips transmission electron microscope (TEM: CM 20/STEM, PW 6060).

The energy-dispersive X-ray diffraction (EDAX) pattern of the glassy particles was also obtained by an EDAX analyzer (Philips TEM-EDAX, PV 9800). For the electron diffraction, the camera length was calibrated experimentally with a gold standard, and an X-ray spectrum analyzer at 200 kV was used.

3.4.3. Laser analysis

To establish the optical properties of doped xerogels, we prepared a sample (<1mm thickness) fabricated with η^6-chromium tricarbonyl(triethoxysilyl)benzene loading of 2.4 % under an acidic sol-gel condition. The thin xerogel film exhibited a nonlinear property. The nonlinear optical (NLO) properties of doped xerogel films were measured by the degenerated into four wave mixing (DFWM) technique. [55] A quartz sample was used as a reference.

We used two types of lasers, a YAG laser with 50 ps pulse-width at 532 nm and a dye laser with 150 fs pulse-width at 640 nm. The output of either of lasers is split into two strong pump beams and a weak probe. The delay between two pump pulses is set to zero to create interference patterns in the doped sol-gel film. Variable delay line on the probe beam allows to measure the decay time of the diffracted beam.

3.5. Results and discussions

Figure 17 describes a sol-gel procedure for the preparations of hexylene-bridged polysilsesquioxanes doped with Cr^o/ CrOx.

The sol-gel process was carried out by a copolymerization of two sol-gel monomers, η6-chromium tricarbonyl(tri-ethoxysilyl)benzene (M-1) and 1,6-bis(triethoxsilyl)hexane (M-2) (Figure 14).

Those sol-gel monomers can be produced bridged Si-O-Si network under either acidic or basic condition, and thus processed into transparent glasses, glassy films, fibers, xerogels, and aerogels, and monoliths. [1,6] From the basic condition, it produced hybrid glasses containing chromium metal particles; because, the M-1 was stable under the basic sol-gel condition.

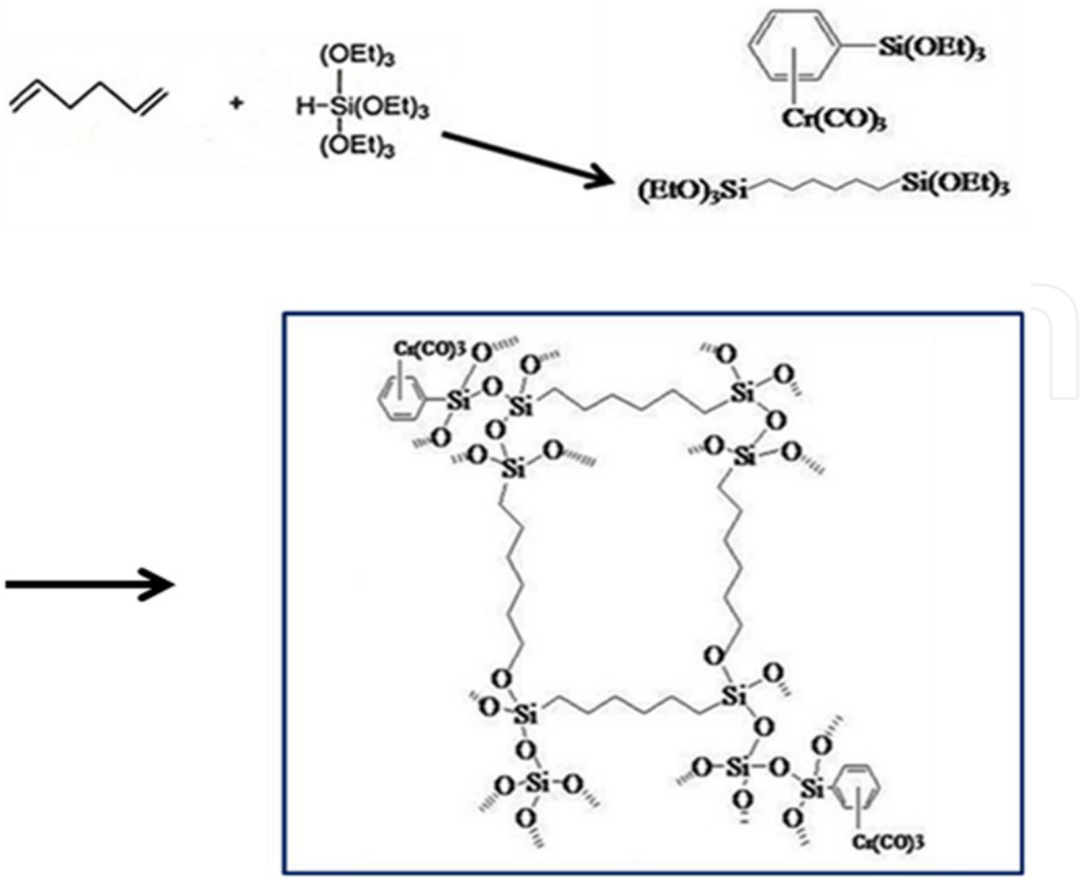

Figure 17. Synthesis of hexylene-bridged xerogel attached with the Cr^{o} precursors.

In contrast, the acid-catalyzed system produced thinner sol-gel films than those of glasses obtained under base condition (Figure 16). Under the acidic sol-gel condition, decomposition of the M-1 competes with sol-gel copolymerization. The product of acid catalyzed decomposition reaction is "chromium oxides" and H_2 (Figure 17). [56-58]

In Figure 18, TEM images of alkylene-bridged silica doped with Cr^{o}/CrOx phases reveal unusual nano-fringe patterns, which rose from the lattice fringes of the aligned alkyl-spacers in the silicate matrix. The novel molecular design results in 'a molecular level grating characteristic' when laser light passes by those periodic carbon-chains (Figure 15).

Based on those nano-fringe patterns, an effective optical grating was created in the hybrid silicate matrix. The TEM images of the doped hybrid glass reveal nano-fringe patterns, which are highly organized nano-periodicity (pointed with arrows in Figure 18). The nano-periodic patterns are sustained over substantial domains and appear to arise from lattice fringes.

In short, the formation mechanism of these nanoperiodic features observed in the TEM images arises from the highly arranged alkylene-spacers in the sol-gel monomer (Figure 15).

EDAX and electron diffraction analyses of these dark regions shown in the TEM images were also performed. In the EDAX spectrum, a Cr (Kα) peak was observed; thus, the dark contrast shown in the TEM images (Figure 18) was identified as a chromium phase spread over the hybrid glassy host by both of EDAX/electron diffraction analyses.

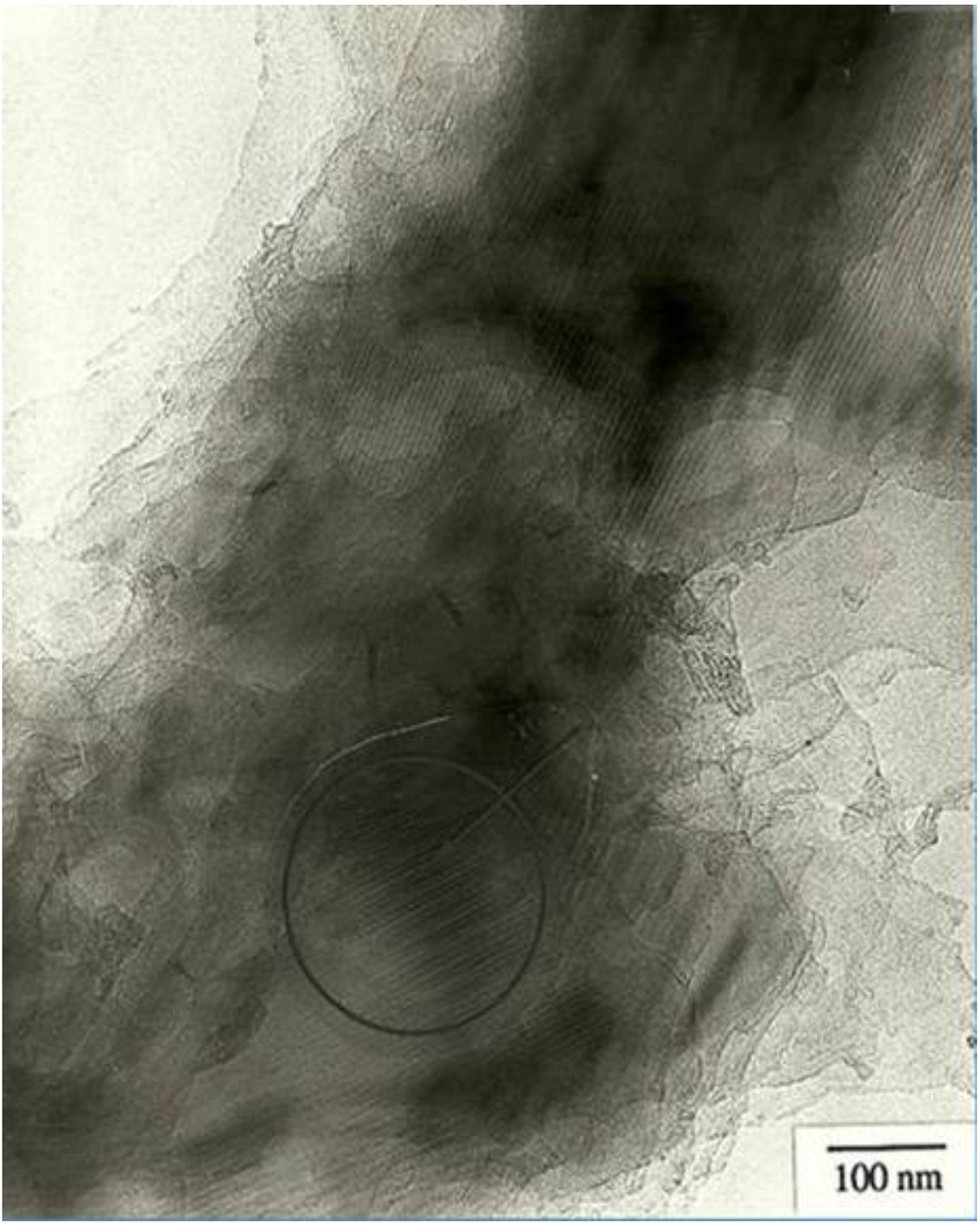

(a)

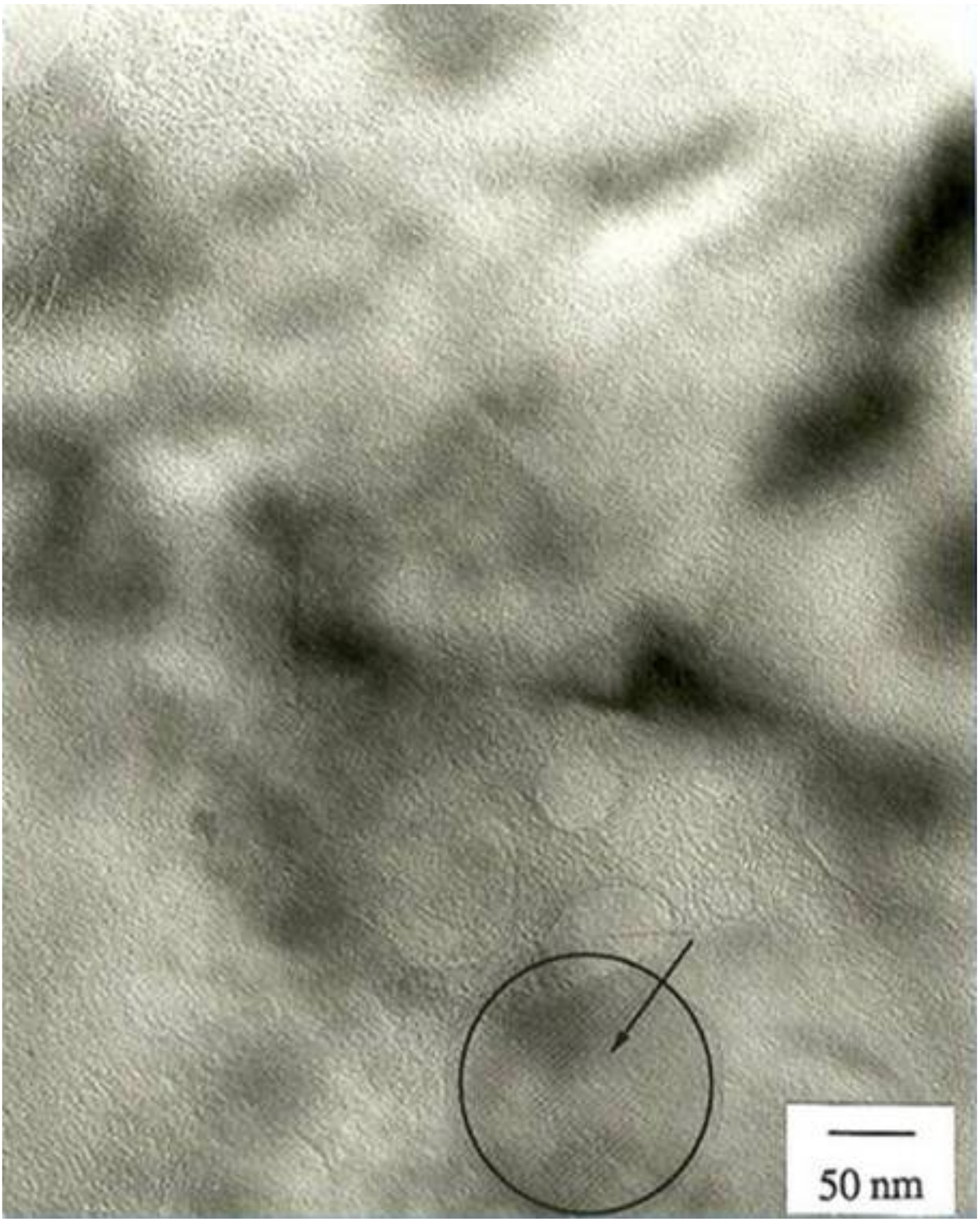

(b)

Figure 18. A and b. TEM Image of Cr^{o}/CrOx-doped hexylene-bridged polysilsesquioxane under acidic condition; it reveals unusual nano-fringe patterns with alternating features of a lattice spacing of about 50 Å in different areas.

The Cr^{o}/CrOx phases were produced by a chemical reaction, which is a simultaneous sol-gel copolymerization then decomposition of the chromium precursor under the acidic condition. The electron diffraction pattern of the dark areas in TEM images was also identified as a mixture of Cr^{o}/ CrOx phases.

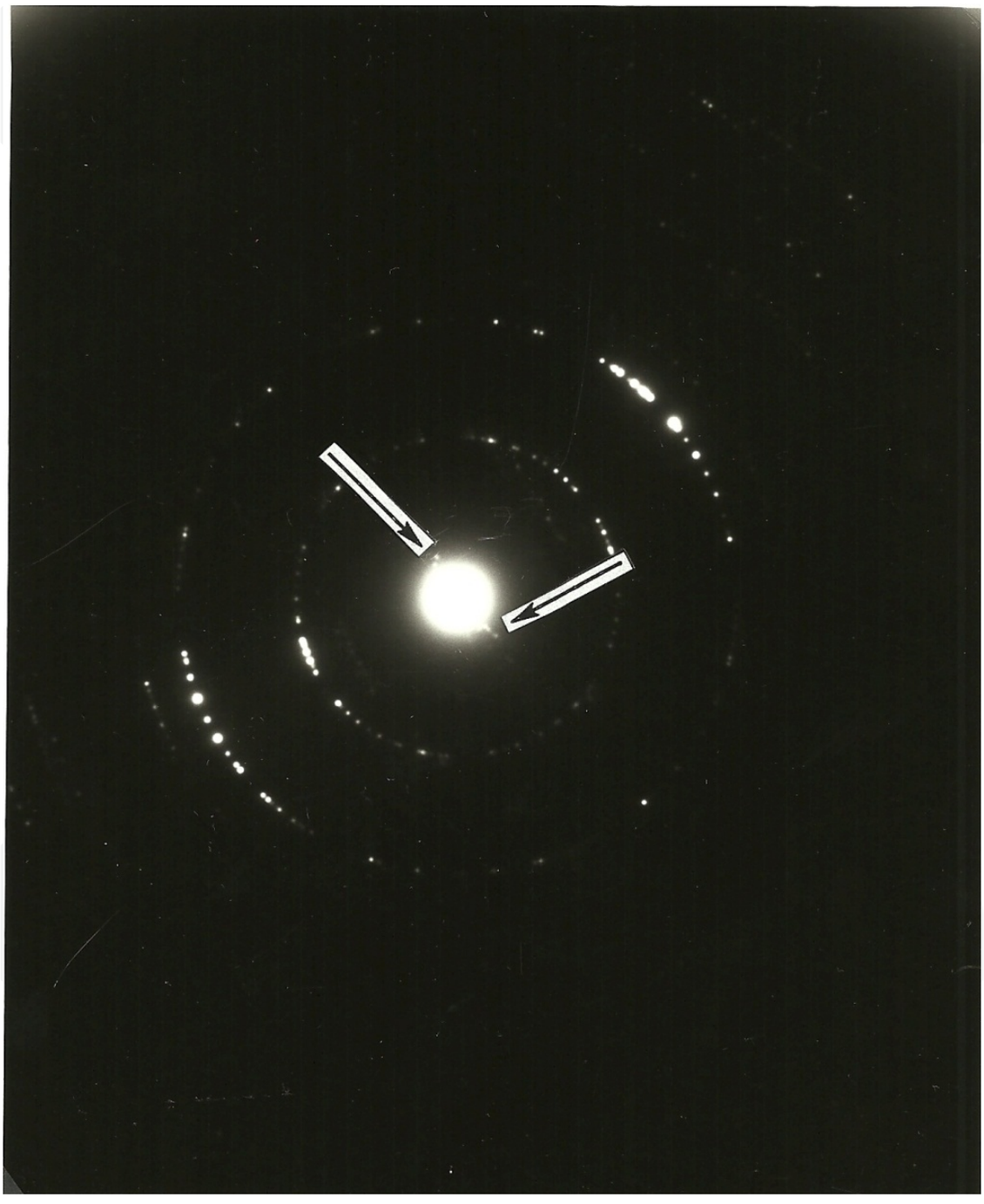

Figure 19. Electron diffraction pattern of doped hybrid glass; circled diffraction patterns correspond to the d-spacings of chromium metal. Highlighted features (arrows) correspond to the nanoperiodicity in the TEM images in Figure 18. From a distance between two diffraction spots point out each arrow a lattice spacing of the nanoscale fringes was calculated to be ~50 Å.

In order to calculate a lattice space of those highly organized nano-fringe patterns shown in the TEM images, we also carried out electron diffraction analysis of the doped sol-gel film. The result is shown in Figure 19. The nano-periodicity gives rise to features in the electron diffraction pattern.

Figure 19 shows the circled diffraction patterns that a rise from crystalline chromium metal and a set of diffractions near the center of the beam corresponded to the nanofringes observed in TEM images (Figure 18).

From the diffraction pattern corresponded to the nano-fringes, a lattice space of the nanostriped patterns observed in TEM images was calculated about 50 Å from a distance between two diffraction spots in two sets of diffraction patterns, which are pointed with arrows in Figure 19; each set consists of two diffraction spots.

The distance between alkyl-spacers significantly relies on the optical grating efficiency, and thus it can be "controlled" by inserting different types and sizes of organic spacers.

As shown in Figure 14, the reactions occurring during the formation of the sol-gel xerogels are complex and include simultaneous sol-gel copolymerization and decomposition of M-1 under the acidic condition. At present, the mechanism of formation of these nanoperiodic features observed in the TEM images may arise from the highly arranged alkyl-spacers in the sol-gel monomer (M-2).

In this study, the nonlinear optical (NLO) properties of the doped xerogel film were measured by the degenerated four wave mixing (DFWM) technique. [12, 13, 55]

In femto- and pico-second experiments, "electronic χ^3" and "population χ^3" of the doped xerogel film have been measured (Figure 20). The DFWM signals for both "pure electronic and population χ^3" are shown in Figure 20 as a small spike around t = 0. It is asymmetric and longer than the laser pulse. The trailing edge of the peak has decay, which is probably connected with population relaxation.

In thermal nonlinearity, the coefficient of phonon diffraction, which is proportional to the coefficient of thermal conductivity, has been calculated from the DFWM experiments as 1.9×10^{-3} cm^2 /sec using an equation, $D = \Lambda^2/4\pi\tau$ (where, Λ is the period of the diffraction grating and τ is the decay time of the thermal signal).

This number is about FIVE times lower than that of a normal glass. In other words, the thermal conductivity of the doped xerogel is FIVE times less than that of a normal glass. In acoustic study, the doped xerogel also shows an interesting new optical property, *an effective generation of a large acoustic wave.*

When the temperature of the doped xerogel at the maximum of the interference pattern goes up, the material expands then a counter propagating wave of expansion and compression start traveling inside the glassy host. Since the index of refraction depends on density of the material, on top of slow decaying thermal grating, we will have *a dynamic diffraction grating propagating with the sound velocity.*

By changing the delay on the laser probe beam, we measured *the period of acoustic grating and extract the sound velocity of the material* (Figure 20). We used YAG laser at 532 nm and 50 ps pulse-width for a laser analysis for the doped xerogel obtained by the novel sol-gel condition, which produces thin xerogel films with unusually high compressibility (higher density).

Small spike around t= 0 corresponds to the signal due to electronic nonlinearlity (Figure 20). The time required for the acoustic wave to travel from one interference maximum to another is twice the time between t=0 and the peak of the acoustic signal. The sound velocity (C) in the thin doped xerogel was calculated from the distance between two acoustic waves ($\Delta\tau$) as $C = 3.2 \times 10^5$ cm/sec.

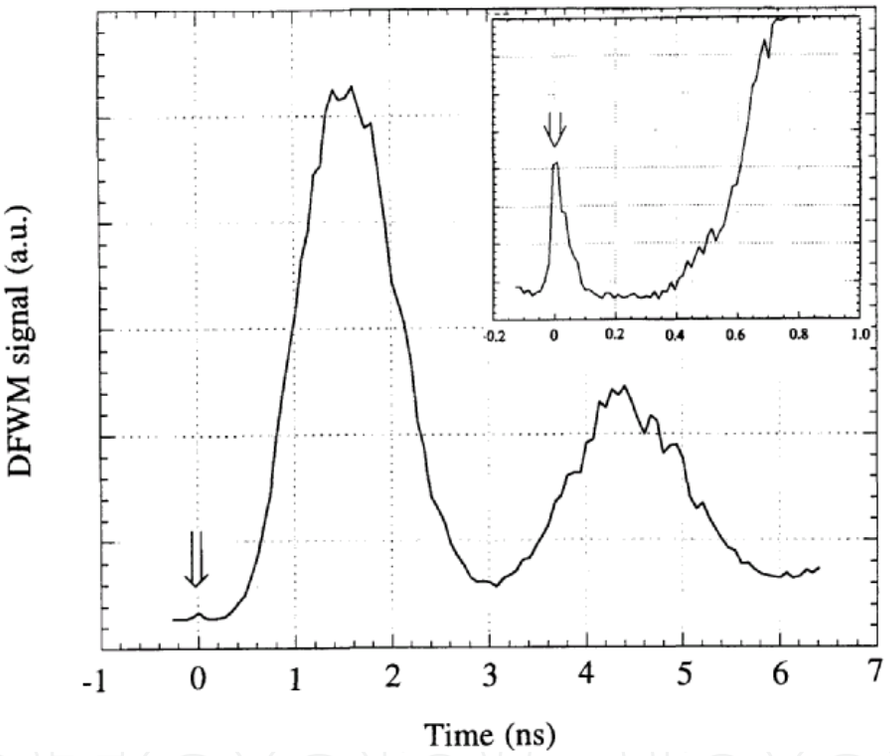

Figure 20. DFWM signals obtained from the doped xerogel measured in femto-second experiment (in a box) and pico-second experiment.

The signal decay time raised from the doped xerogel film was evaluated by the continuous wave (CW) probe experiment (Figure 21); it was obtained as 17 μsec.

Therefore, the doped xerogel serves as a heat generator in the slow nonlinearities due to the low thermal conductivity and high compressibility of the hybrid glass, thus the heat is transferred into expansion or compression wave (acoustic wave) very efficiently.

We also measured the diffraction efficiency of the probe beam at the delay time, corresponding to the peak of acoustic signal. At energy level about P = 0.47 J/cm^2, which is close to the optical damage threshold, the diffraction efficiency was 45 %.

The amplitude of the acoustic signal will depend upon how effectively the laser pulse energy is transferred to an expansion wave, which in turn depends on compressibility of the host materials. For a comparison we did the same measurement for a dye solution in methanol with the same optical density and the same energy density. The diffraction efficiency of methanol was 25 %, which means the compressibility of the doped xerogel film is as effective as liquid.

In a conclusion from the laser experiments, the doped xerogel film has a lower thermal conductivity than that of a normal glass. The compressibility of the doped xerogel is sufficiently high so the density grating formed in the doped xerogel could be effective to create high diffraction beam in the sound velocity.

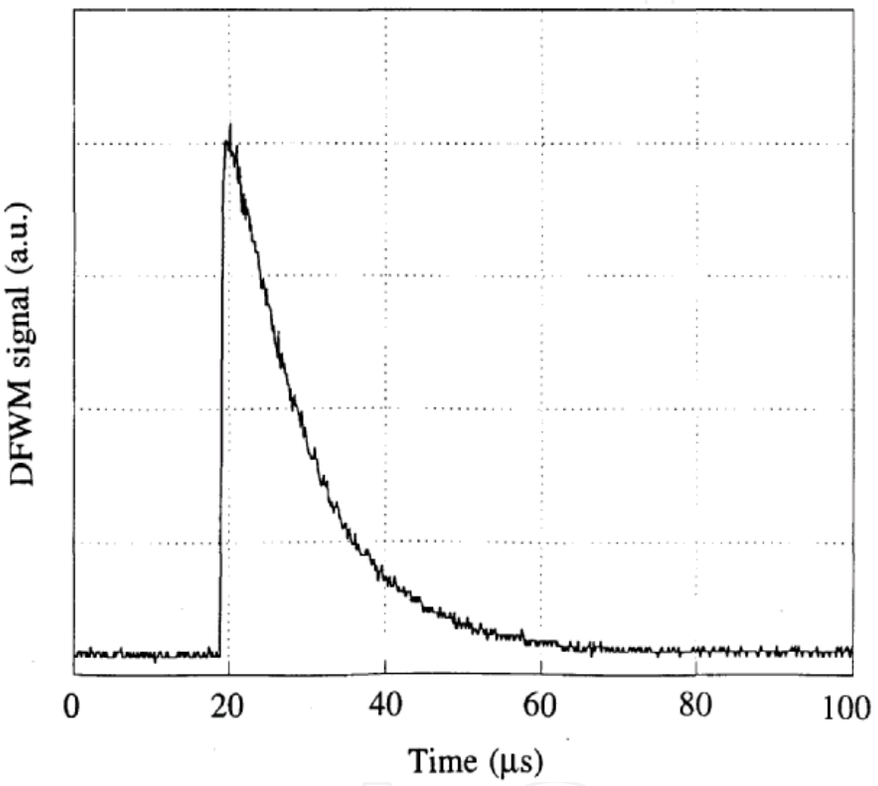

Figure 21. The decay of thermal signal for the doped xerogel measured in CW probe experiment.

We also believe that the nano-fringe patterns revealed in the TEM images (Figure 18), which rose from the lattice fringes of alkylene-bridged silicate matrix may result in an effective grating characteristics when the light passes by those long carbon-chains of alkylene-based polymeric networks.

The characteristics observed from the novel doped xerogel are new photonic properties, which hitherto have not been possible from simple physical mixing process of individual components at the bulk scale. In other words, those new optical properties are created by *the molecular-level hybridization*.

Based on these experiments, the (Cr^{o}/CrOx)-doped polysilsesquioxane with low thermal conductivity and high compressibility are suggested as a new type of optical device materials for optical applications, for example diffraction beam modulators.

We demonstrated here some examples of creating new optical properties by designing novel molecular building blocks at the molecular-scales via *the molecular-level hybridization.*

4. Conclusions

We introduce the *molecular-level hybridization* for the preparation of polysilsesquioxanes, which are hybrids of inorganic oxides and organic network polymers.

Optically transparent hybrid glasses are prepared by a molecular tailoring technique, which produces sol-gel processible monomers.

The resulting hybrid glasses show novel optical properties, which would not be expected from those individuals by the loss of individuals' identities after the molecular-level mixing process, thereby creating entirely new properties.

Author details

Kyung M. Choi
University of California at Irvine, USA

5. References

[1] Brinker, J. & Scherer, G. W. (1990) *Sol-Gel Science: The Physics and Chemistry of Sol-Gel Processing:* Published by Academic Press, Inc.
[2] Shea, K. J., Loy, D. A., & Webster, O. W. (1989) *Chem. Mater.,* 1, 572.; Shea, K. J., Loy, D. A., & Webster, O. W. (1992) *J. Am. Chem. Soc.,* 114, 6700.
[3] Corriu, R. J. P., Moreau, J. J. E., Thepot, P., & Wong, C. M. M. (1992) *Chem. Mater.,* 4, 1217; Corriu, R. J. P., Thepot, P., & Mang, M. W. C. (1994) *J. Mater. Chem.,* 4, 987.
[4] Loy, D. A. & Shea, K. J. (1995) *Chem. Rev., 95* (5), 1431.
[5] Cerveau, G., Corriu, R. J. P., & Lepeytre, C. (1997) *J. Orgmetal. Chem.,* 548 (1), 99.
[6] Choi, K. M. & Shea, K. J. (1998) *Photonic Polymer Systems, Fundamentals, Methods, and Application*: Edited by D. L. Wise et al. World Scientific Publishing Co. Pte. Ltd.
[7] Shea, K. J. & Loy, D. A. (2001) *MRS Bulletin*, 26, 368.
[8] Loy, D. A. & Rahimian, K. (May 2003), *Handbook of Organic-Inorganic Hybrid Materials and Nanocomposites*: Edited by Hari Singh Nalwa Formerly of Hitachi Research Laboratory, Hitachi Ltd.
[9] Shea, K. J., Moreau, J., Loy, D. A., Corriu, R.J.P., & Bour, B. (2003) *Hybrid Materials*: Published by Wiley Inter science, New York.
[10] Zhao, L., Vaupel, M., Loy, D. A., & Shea, K. J. (2008) *Chem. Mater.,* 20, 1870.
[11] Oviatt, H. W. Jr., Shea, K. J., & Small, J. H. (1993) *Chem. Mater.* , 5, 943.
[12] Oviatt, H. W., Shea, K. J., Kalluri, S., Shi, Y., Steier, W. H., & Dalton, L. R. (1995) *Chem. Mater.,* 7, 493.
[13] Dalton, L. R. (1998) *Polymers for Electro-Optic Modulator Waveguides in Electrical and Optical Polymer Systems; Fundamentals, Methods, and Applications*: Edited by Wise, D. L.,

Copper, T. M., Gresser, J. D., Trantolo, D. J., & Wnek, G. E., (World Scientific, Singapore) Chapter 18.
[14] Walcarius, A. (2001) *Chem. Mater., 13* (10), 3351.
[15] Matsubara, I. (2003) *AIST Today* , 3 (8), 32.
[16] Schaefer, D. W., Beaucage, G., Loy, D.A., Shea, K. J., & Lin, J.S. (2004) *Chem. Mater.,* 16, 1402.
[17] Pang, Y.X., Hodgson, S.N.B., Koniarek, J., & Weglinski, B. (2006) *J. of Magnetism and Magnetic Mater.,* 301(1), March 27, 83.
[18] Choi, K. M. & Shea, K. J. (1993*) Chem. Mater.,* 5, 1067.
[19] Choi, K. M. & Shea, K. J. (1994) *J. Phys. Chem.,* 98, 3207.
[20] Choi, K. M. & Shea, K. J. (1994) *J. Am. Chem. Soc.,* 116, 9052.
[21] Choi, K. M., Hemminger, J. C., & Shea, K. J. (1995) *J. Phys. Chem.,* 99, 4720.
[22] Choi, K. M. & Shea, K. J. (1995) *J. of Sol-Gel Sci. Tech.,* 5, 143.
[23] Choi, K. M. & Rogers, J. A. (2003) *J. Am. Chem. Soc.,* 125, 4060.
[24] Choi, K. M. (2005) *J. Phys. Chem. B,* 109, 21525.
[25] Choi, K. M. (2007) *Mater. Chem. Phys.,* 103, 176.
[26] Choi, K. M. & Shea, K. J. (2008) *J. Phy. Chem. C,* 112, 18173.
[27] Carpenter, J. P., Lukehart, C. M. , Stock, S. R., & Wittig, J. E. (1995) *Chem. Mater.,* 7, 201.
[28] Pocard, N. L., Alsmeyer, D. C., McCreery, R. L., Neenan, T. X., & Callstrom, M. R. (1992) *J. Am. Chem. Soc.,* 114, 769.
[29] Kim, J.H. & Holloway, P. H. (2005) *Adv. Mater.,* 17, 91.
[30] Xia, H. R., Lu, G. W., Zhao, P., Sun, S. Q., Meng, X. L., Cheng, X. F., Qin, L. J., Zhu, L., & Yang, Z. H. (2005) *J. Mater. Res.,* 20, 30.
[31] Mukhopadhyay, S., Ramesh, K. P., Kannan, R., & Ramakrishna, J. (2004) *Phys. Rev. B: Cond. Matter Mater. Phys.,* 70, 224202.
[32] Dantelle, G., Mortier, M., Vivien, D., & Patriarche, G. (2005) *J. Mater. Res.*, 20. 472.
[33] Xiao, S., Yang, X., Liu, Z., & Yan, X. H. (2004) *J. Appl. Phys.*, 96. 1360.
[34] Buscaglia, M. T., Buscaglia, V., Ghigna, P., Viviani, M., Spinolo, G., Testino, A., & Nanni, P. (2004) *Phys. Chem. Chem. Phys.,* 6, 3710.
[35] Stepanov, S., Hernandez, E., & Plata, M. (2004) *Opt. Lett.,* 29, 1327.
[36] Lin, H., Jing, S., Wu, J., Song, F., Peyghambarian, N., & Pun, E.Y.B. (2003) *J. Phys. D: Appl. Phys.,* 26, 812.
[37] Sohler, W. & Suche, H. (2000) *Opt. Eng.,* 66, 127.
[38] Neuman, W., Pennington, D., Dawson, J., Drobshoff, A., Beach, R., Jovanovic, I., Liao, Z., Payne, S., & Barty, C.P.J. (2005) *Proc. SPIE Int. Soc. Opt. Eng.* , 5653, 262.
[39] Huang, X., Liu, Y., Sui, Z., Li, M., Lin, H., Wang, J., Zhao, D., Wang, F., & Chen, J. (2005) *Proc. SPIE Int. Soc. Opt. Eng.*, 5623, 679.
[40] Sanchez, C., Lebeau, B., Chaput, F., & Boilot, J. P. (2003) *Adv. Mater.* , 15. 1969.
[41] Shea, K. J. & Loy, D. A. (2001) *Chem. Mater.* , 13, 3306.
[42] Schmidt, H. (1989) *Sol–Gel Science and Technology:* Published by World Scientific, Singapore.
[43] Urquhart, P. (1988) *IEEE Proc.-J.; Optoelectronics*, 135, 385.
[44] Murray, C. B., Kagan, C. R., & Bawendi, M. G. (1995) *Science,* 270, 1335.

[45] Empedocles, S. A., Norris, D. J., & Bawendi, M. G. (1996) *Phys. Rev. Lett.,* 77, 3873.
[46] Armelao, L., Gross, S., Obetti, G., & Tondello, E. (2004) *Surf. Coat. Technol.,* 109, 218.
[47] Di Giovanni, D. J. (1992) *Mater. Res. Soc. Proc.,* 244, 135.
[48] Rossetti, R., Hull, R., Gibson, J. M., & Brus, L. E. (1985) *J. Chem. Phys.,* 82 (l), 552; Zhang, Y., Raman, N., Bailey, J. K., Brinker, C. J., & Crooks, R. M. (1992) *J. Phys. Chem.,* 96, 9098.
[49] Schmid, G. (1992) *Chem. Rev.,* 92, 1709.
[50] Grate, J. W., Kaganove, S. N., Patrash, S. J., Craig, R., & Bliss, M. (1997) *Chem. Mater., 9* (5), 1201.
[51] Ponson, L., Boechler, N., Lai, Y. M., Porter, M. A., Kevrekidis, P. G. , & Daraio, C. (2010) *Physical Review E*, 82, 021301.
[52] Spadoni, A. & Daraio, C. (2010) *Proc. Natl. Acad. Sci. USA*, 107, 7230.
[53] Porter, M.A., Daraio, C., Herbold, E.B., Szelengowicz, I., & Kevrekidis, P.G. (2008) *Physical Review E*, 77, 015601(R).
[54] Sullivan, P. A., Olbricht, B. C., & Dalton, L. A. (2008) *Journal of Lightwave Technology*, 26 (15), 2345.
[55] Ma, H., Chen, B., Takafumi, S., Dalton, L. R., & Jen, A. K.-Y. (2001) *J. Am. Chem. Soc.* , 123, 986.
[56] η^6-Bisarene chromium complexes decompose in dilute acid. Oxidation and disproportion products (of both organic and Cr) are observed. [57] η^6-Arene $Cr(CO)_3$ complexes form adducts with Lewis and protonic acids but their decomposition products have not been investigated. [58]
[57] Gribov, B. G., Mozzhukhin, D. D., Kozyrkin, B. I., & Strizhkova, A. S. (1972) *J. Gen. Chem. USSR (Eng. Transl.),* 42, 2521.
[58] Flood, T. C., Rosenberg, E., & Sarhangi, A. (1997) *J. Am. Chem. Soc.,* 99, 4334; Lillya, C. P. & Sahatjian, R. A. (1972) *Inorg. Chem.,* 11, 889.